Exceptional Thermal Stability of Lanthanide-Phosphonate Frameworks

by

Ana D. G. Firmino,[a,b] Ricardo F. Mendes,[a,*] Flávio Figueira,[a]

João P. C. Tomé,[c] Filipe A. Almeida Paz[a,*]

[a] *Department of Chemistry, CICECO – Aveiro Institute of Materials, University of Aveiro, 3810-193 Aveiro, Portugal*

[b] *LAQV-REQUIMTE, Department of Chemistry, University of Aveiro, 3810-193 Aveiro, Portugal*

[c] *Centro de Química Estrutural, Instituto Superior Técnico, University of Lisbon, Avenida Rovisco Pais, 1049-001 Lisbon, Portugal*

* *To whom correspondence should be addressed:*

Filipe A. Almeida Paz

Department of Chemistry, CICECO – Aveiro Institute of Materials

University of Aveiro

3810-193 Aveiro

Portugal

E-mail: filipe.paz@ua.pt

Telephone: (+351) 234 401418

Table of Contents

1. Experimental Section

1.1. General Instrumentation

Scanning Electron Microscopy (SEM) images were acquired using either a Hitachi S4100 field emission gun tungsten filament instrument operating at 25 kV or a high-resolution Hitachi SU-70 operating at 4 kV. Samples were prepared by deposition on aluminum sample holders, followed by carbon coating using an Emitech K950X carbon evaporator.

Energy-dispersive X-ray spectroscopy (EDS) data and SEM mapping images were recorded using the aforementioned microscope operating at 15 kV and either a Bruker Quantax 400 or Esprit 1.9 EDS microanalysis system.

Thermogravimetric analyses (TGA) were carried out using a Setaram Instrumentation SETSYS Evolution, from ambient temperature to *ca.* 1200 ºC (heating rate of 10 ºC/min), under a continuous stream of O_2 at a flow rate of 200 mL/min.

Fourier Transform Infrared (FT-IR) spectra (in the range 4000-350 cm^{-1}) were recorded as KBr pellets (*ca.* 2 mg of sample was mixed in a mortar with 200 mg of KBr) using a Bruker Tensor 27 spectrometer by averaging 256 scans at a maximum resolution of 2 cm^{-1}.

Elemental analyses for C and H were performed with a Truspec Micro CHNS 630-200-200 elemental analyzer at the Department of Chemistry, University of Aveiro. The analysis parameters were as follows: sample amount between 1 and 2 mg; combustion furnace temperature = 1075 ºC; afterburner temperature = 850 ºC. Detection method: carbon and hydrogen – infrared absorption. Analysis time = 4 minutes. Required gases: carrier, helium; combustion, oxygen; pneumatic, compressed air.

Routine Powder X-Ray Diffraction (PXRD) data for all prepared materials were collected at ambient temperature using an Empyrean PANalytical diffractometer (Cu K$\alpha_{1,2}$ X-radiation, λ_1 = 1.540598 Å; λ_2 = 1.544426 Å) equipped with a PIXcel 1D detector and a flat-plate sample holder in a Bragg-Brentano para-focusing optics configuration (45 kV, 40 mA). Intensity data were collected using the step-counting method (step 0.01º), in continuous mode, in the *ca.* $3.5 \leq 2\theta^{o} \leq 50^{o}$ range.

Variable-temperature powder X-ray diffraction data were collected on a PANalytical X'Pert Powder diffractometer (Cu K$\alpha_{1,2}$ X-radiation, λ_1 = 1.540598 Å; λ_2 = 1.544426 Å) under an air atmosphere, equipped with a PIXcel 1D detector, flat-plate sample holder in a Bragg-Brentano para-focusing optics configuration (40 kV, 50 mA), and high-temperature Anton Paar HKL 16 chamber controlled by an Anton Paar 100 TCU unit. Intensity data were collected in the continuous mode (*ca.* 100 s data acquisition) in the angular range *ca.* $5 \leq 2\theta^{o} \leq 35$.

1.2. Reagents and Solvents

[1,1'-Biphenyl]-3,3',5,5'-tetrayltetrakis(phosphonic acid) (H_8btp) was prepared using the optimized procedure previously reported by us.[1, 2] All other chemicals, including solvents, were readily available from commercial sources and were used as received without further purification: lanthanide(III) chloride hexahydrates ($LnCl_3 \cdot 6H_2O$, Ln^{3+} = Gd^{3+}, Tb^{3+}, Dy^{3+}, Ho^{3+}, Er^{3+} and Tm^{3+}, 99.9%, Sigma-Aldrich); copper(II) chloride dihydrate ($CuCl_2 \cdot 2H_2O$, extra pure, Riedel); 3,5-dibromophenylboronic acid ($C_6H_5BBr_2O_2$, containing varying amounts of anhydride, TCI); 1,10-phenanthroline monohydrate ($C_{12}H_{10}N_2O$, >99.0%, TCI); sodium hydroxide (NaOH, ≥98%, Sigma-Aldrich); triethyl phosphate ($C_2H_5PO_3$, 98%, Sigma-Aldrich); tetrakis(triphenylphosphine)-palladium(0) ($Pd[(C_6H_5)_3P]_4$, 99%, Sigma-Aldrich); hydrochloric acid (HCl, 37%, José Manuel Gomes dos Santos Lta.); dichloromethane (CH_2Cl_2), pure, Sigma-Aldrich); methanol (CH_4O, >99.8%, Fluka); n-hexane (C_6H_{14}, >99%, Sigma-Aldrich); propan-2-ol (C_3H_8O, 99,7%, Carlo Erba Reagents); deuterated dimethyl sulfoxide (DMSO-d_6, 99,99%, Euriso-top); deuterated chloroform ($CDCl_3$, 99,99%, Euriso-top); potassium bromide (KBr for infrared spectroscopy, > 99%, BDH SpectrosoL).

1.3. Synthesis of [1,1-biphenyl]-3,3´,5,5´-tetrayltetrakis(phosphonic acid) (H_8btp)

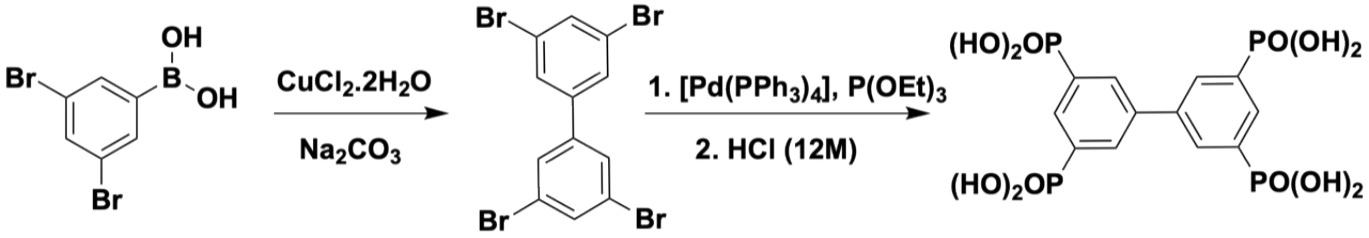

Scheme S1 Preparation of [1,1-biphenyl]-3,3´,5,5´-tetrayltetrakis(phosphonic acid) (H_8btp).

Synthesis of 3,3´,5,5´-tetrabromo-1,10-biphenyl: Dibromo-arylboronic acid (2.0 g, 7.2 mmol), $CuCl_2 \cdot 2H_2O$ (48.0 mg, 0.36 mmol, 5 mol%), Na_2CO_3(99.9 mg, 0.71 mmol, 10 mol%), methanol (20 mL) were added to a round bottom flask. The reaction mixture was stirred at 25 °C for 5h and monitored using TLC. The reaction was then quenched with 10 mL H_2O, extracted with 3 × 20 mL ethyl acetate, and the organics were dried over a pad of $NaSO_4$.

^{1}H NMR (300 MHz, $CDCl_3$) δ 7.69 (t, J = 1.7 Hz, 2H), 7.59 (d, J = 1.7 Hz, 4H).

^{13}C NMR (75 MHz, $CDCl_3$) δ 141.7, 133.9, 128.9, 123.5.

Synthesis of Octaethyl-[1,10-biphenyl]-3,3´,5,5´-tetrayltetrakis(phosphonate): $[Pd(PPh_3)_4]$ (0.060 g, 0.014 mmol) and triethylphosphite (8 mL, 12 mmol) were added to a 35 mL IntelliVent microwave reactor

containing 3,3′,5,5′-tetrabromo-1,10 -biphenyl (1.01 g, 2.14 mmol). The vial was placed inside a CEM Focused Microwave Synthesis System Discover S-Class equipment, pre-stirred for 1 min, and irradiated for 20 min (230 ºC, 300 W, 100 psi). A constant flow of air (*ca.* 20-30 psi of pressure) ensured close control of the temperature inside the reactor. The resulting mixture was monitored by TLC and purified by flash column chromatography using a mixture of CH_2Cl_2/MeOH (95:5 v/v). The resulting oily residue was washed with hexane (50 mL). Octaethyl-[1,10-biphenyl]-3,3′,5,5′-tetrayltetrakis(phosphonate) was obtained as a colorless oil in 95% yield.

^{1}H NMR (300 MHz, $CDCl_3$) δ 8.35 – 8.14 (m, 6H, Ar-H), 4.29 – 4.10 (m, 16H, C$\underline{H}_2$), 1.37 (t, J = 7.1 Hz, 24H, C$\underline{H}_3$).

^{31}P NMR (121 MHz, $CDCl_3$) δ 15.57 (m, 4P).

^{13}C NMR (75 MHz, $CDCl_3$) δ 139.9 (t, J = 8.7 Hz), 134.5-134.1 (m, 6 C), 130.6 (dd, J = 113.6 Hz, and 8.7 Hz, 4 C, $\underline{C}PO_3Et_2$), 62.7 ($\underline{C}H_2CH_3$), 16.4 ($CH_2\underline{C}H_3$).

Synthesis of [1,1-biphenyl]-3,3′,5,5′-tetrayltetrakis(phosphonic acid) (H_8btp): H_8btp was prepared as previously reported, with some minor modifications. A mixture composed of octaethyl-[1,10-biphenyl]-3,3′,5,5′-tetrayltetrakis(phosphonate) (1.12 g, 1.57 mmol) and concentrated HCl (30 mL) was refluxed under continuous magnetic stirring for approximately 24 h. After cooling to ambient temperature, distilled water was added and the solvents were evaporated under reduced pressure. The target compound, [1,1-biphenyl]-3,3′,5,5′-tetrayltetrakis(phosphonic acid), was washed with acetone (20 mL) and isolated as a white powder.

^{1}H NMR (300 MHz, DMSO-d_6) δ 8.09 – 8.00 (m, 6H).

^{31}P NMR (121 MHz, DMSO-d_6) δ 10.80 (m, 4P).

^{13}C NMR (75.47 MHz, DMSO-d_6): δ 137.9 (t, J = 13.6 Hz, 2C), 136.46 (d, J = 13.0 Hz, 4 C, $\underline{C}PO_3H_2$), 134.09 (d, J = 13.0 Hz, 2C), 132.18 (d, J = 9.8 Hz, 4C).

1.4. Synthesis of [Ln(H_5btp)]·2H_2O (1)

Synthesis was performed as previously reported by our research group, with small differences as described below.[2]

Reactive mixtures composed of 0.1002 g of lanthanide(III) oxides [Ln_2O_3, where Ln^{3+} = Gd^{3+} (**1Gd**), Tb^{3+} (**1Tb**), Dy^{3+} (**1Dy**), Ho^{3+} (**1Ho**), Er^{3+} (**1Er**), and Tm^{3+} (**1Tm**)], and 0.025 g of [1,1'-biphenyl]-3,3',5,5'-tetrayltetrakis(phosphonic acid) (H_8btp), with an overall molar ratio of approximately 1:4 (H_8btp: Ln^{3+}), were individually prepared in a mixture of distilled water, HCl (6 M), and methanol (2 mL each solvent). Mixtures

were kept under constant magnetic stirring in open air and ambient temperature for approximately 15 min. The resulting homogeneous suspensions were transferred to Teflon-lined Parr Instrument reaction vessels and placed inside a MMM Venticell oven. The heating program included: i) heating for 48 h up to 140 ºC, ii) 24 h upholding at 140 ºC, and iii) cooling over a period of 48 h to ambient temperature. The resulting materials were isolated as white microcrystalline powders, recovered by vacuum filtration, washed with abundant amounts of distilled water and dried at ambient temperature.

Elemental CH composition (%):

Calcd for **1Gd**: C 21.7; H 2.28. Found: C 22.1; H 2.44.

Calcd for **1Tb**: C 21.6; H 2.27. Found: C 21.2; H 2.36.

Calcd for **1Dy**: C 21.5; H 2.26. Found: C 22.0; H 2.41.

Calcd for **1Ho**: C 21.4; H 2.25. Found: C 21.5; H 2.35.

Calcd for **1Er**: C 21.4; H 2.24. Found: C 21.5; H 2.37.

Calcd for **1Tm**: C 21.3; H 2.24. Found: C 21.6; H 2.10.

Thermogravimetric analysis (TGA) data (weight losses in %) and derivative thermogravimetric peaks (DTG, in italics in parentheses)

1Gd: 25-250 ºC -3.82% (*72 ºC*); 250-670 ºC -4.61% (*355 ºC*); 670-890ºC-6.66% (*835 ºC*); 890-1200 ºC-13.91% (*951ºC*). Total loss: 29.0%.

1Tb: 25-245 ºC -4.83% (*67 ºC*); 245-650 ºC -6.05% (*353 ºC*); 650-867 ºC -7.69% (*838 ºC*); 867-1200 ºC -12.37% (*945ºC*). Total loss: 30.9%.

1Dy: 25-220 ºC -5.11% (*69 ºC*); 220-650 ºC -5.97% (*349 ºC*); 650-865 ºC -5.79% (*841 ºC*); 865-921 ºC -4.76% (*897 ºC*); 921-1200 ºC -15.47% (*948ºC*). Total loss: 37.1%.

1Ho: 25-230 ºC -4.53% (*65 ºC*); 230-650 ºC -6.01% (*354 ºC*); 650-835 ºC -3.77% (*825 ºC*); 835-937 ºC -11.90% (*920 ºC*); 937-1200 ºC -7.68% (*950ºC*). Total loss: 33.9%.

1Er: 25-245 ºC -5.57% (*70 ºC*); 245-650 ºC -6.32% (*355 ºC*); 650-865ºC-6.11% (*835 ºC*); 865-1200 ºC-17.53% (*951ºC*). Total loss: 35.5%.

Selected FT-IR data (in cm^{-1}; from KBr pellets):

1Gd: $\nu(H_2O_{cryst}$ + POH + C–H) = 3550-2540*br*; ν(C=C) + $\delta(H_2O)$ = 1720-1560*m*; ν(P=O) = 1230-1040*vs*; ν(P–O) = 965-845*vs*; ν(P–C) = 696*m*.

1Tb: $\nu(H_2O_{cryst}$ + POH + C–H) = 3590-2490*br*; ν(C=C) + $\delta(H_2O)$ = 1720-1560*m*; ν(P=O) = 1260-975*vs*; ν(P–O) = 975-860*vs*; ν(P–C) = 697*m*.

1Dy: $\nu(H_2O_{cryst}$ + POH + C–H) = 3565-2500*br*; ν(C=C) + $\delta(H_2O)$ = 1710-1575*m*; ν(P=O) = 1230-975*vs*; ν(P–O) = 975-840*vs*; ν(P–C) = 697*m*.

1Ho: $\nu(H_2O_{cryst} + POH)$ = 3535-2510*br*; ν(C=C) + $\delta(H_2O)$ = 1700-1580*m*; ν(P=O) = 12301015*vs*; ν(P–O) = 970-860*vs*; ν(P–C) = 698*m*.
1Er: $\nu(H_2O_{cryst} + POH)$ = 3580-2500*br*; ν(C=C) + $\delta(H_2O)$ = 1690-1570*m*; ν(P=O) = 12351015*vs*; ν(P–O) = 978-865*vs*; ν(P–C) = 698*m*.
1Tm: $\nu(H_2O_{cryst} + POH)$ = 3525-2500*br*; ν(C=C) + $\delta(H_2O)$ = 1710-1570*m*; ν(P=O) = 1270975*vs*; ν(P–O) = 975-835*vs*; ν(P–C) = 697*m*.

1.5. Synthesis of [Ln(L)(HL)] (1Tb_dry)

These materials were obtained by the dehydration of $[Ln(H_5btp)]\cdot 2H_2O$ (**1**). Each compound (200 mg) was placed in an open crucible inside an oven, preheated to 400 °C, and dehydrated overnight. The resulting grey powder was recovered and cooled to ambient temperature.

Selected FT-IR data (in cm^{-1}; from KBr pellets) for [Tb(L)(HL)] (1Tb_dry): ν(C–H) = 3090-3015*vs*; ν(C=C) = 1625-1570*vs*; ν(P=O) = 1260-1030*vs*; ν(P–O) + ν(P–O–P) = 1055-930*vs*; ν(P–C) = 695*m*.

1.6. Single-Crystal X-ray Diffraction Studies

The inspection of various batches of microcrystalline powders isolated from the dried material at 400 ºC was performed using a Stemi 2000 stereomicroscope equipped with Carl Zeiss lenses. This allowed the identification of long white needles (dimensions of about 0.06×0.02×0.01 mm) which were studied using single-crystal X-ray diffraction. Needles were manually selected and immersed in FOMBLIN Y perfluoropolyether vacuum oil (LVAC 140/13, Sigma-Aldrich).[3] Crystals were mounted on Hampton Research CryoLoops and preliminary X-ray diffraction data were collected at 150(2) K on a Bruker D8 QUEST equipped with a Mo Kα sealed tube (λ = 0.71073 Å), a multilayer TRIUMPH X-ray mirror, a PHOTON 100 CMOS detector, and an Oxford Instruments Cryostrem 700+ Series low temperature device. The instrument was controlled with the APEX2 software package.[4]

The isolated crystalline material of [Tb(L)(HL)] (**1Tb_dry**) was of very poor quality being composed mostly of powder. The crystals were obtained by calcination at 400 ºC leading to the formation of highly cracked crystals with large defects. The few selected single crystals that could be hand picked exhibited a very poor overall diffraction, with scattered (many times overlapped) reflections, preventing even the normal indexing procedures of the crystal. This strategy was thus based on the data collection of a full sphere of reflections for the selected crystal. Reflections were only visible up to *ca.* 1.6 Å resolution, resulting in low data completion of approximately 78.1%. The collected diffraction images were processed using the software package SAINT+,[5] and data were corrected for absorption by the multi-scan semi-empirical method implemented in SADABS.[6] The crystal structure of **1Tb_dry** was solved using the algorithm implemented in SHELXT-2014,[7,8] which allowed the immediate location of almost all of the heaviest atoms composing the

asymmetric unit of the material. Non-hydrogen atoms could be however + refined by assuming anisotropic models. The backbone was instead included in the final structural model by using individual isotropic parameters for each atom.

Hydrogen atoms bound to carbon were placed at their idealized positions using the *HFIX 43* in SHELXL-2014, which were included in subsequent refinement cycles with isotropic displacement parameters (U_{iso}) fixed at 1.2×U_{eq} of the parent carbon atoms. Hydrogen atoms associated with the terminal –POH group were placed according to the environment of the terminal oxygen atom and P–O distances. It is noteworthy that to determine which groups should be protonated it was necessary to simultaneously take into account the P–O bond lengths and the possibility of forming hydrogen bonds with neighbouring moieties. The sole atom was placed at a calculated position using the *HFIX 83* instruction in SHELXL-2014 and was refined assuming an isotropic thermal displacement parameter (U_{iso}) fixed at 1.5×U_{eq} of the parent oxygen atom.

The last difference Fourier map synthesis showed the highest peak (3.334 eÅ^{-3}) and the deepest hole (-1.828 eÅ^{-3}) located at 1.82 and 1.17 Å from O2 and O3, respectively. Structural refinements were performed using the graphical interface ShelXle.[9] Structural drawings have been created using the software package Crystal Impact Diamond.[10] Information concerning crystallographic data collection and structure refinement details is summarized in Table S1. Tables S2 and S3 list the most significant geometrical parameters of the crystallographically independent Tb^{3+} coordination sphere and hydrogen bonding geometry.

Crystallographic data (including structure factors) for the crystal structure of **1Tb_dry** have been deposited with the Cambridge Crystallographic Data Centre as supplementary publication data No. 2362876. Copies of the data can be obtained free of charge on application to CCDC, 12 Union Road, Cambridge CB2 2EZ, U.K. FAX: (+44) 1223 336033. E-mail: deposit@ccdc.cam.ac.uk.

Table S1. Crystal data collection and structure refinement details for [Tb(L)(HL)] (**1Tb_dry**).

Formula	$C_{12}H_7O_{10}P_4Tb$
Formula weight	593.98
Temperature / K	150(2)
Crystal system	Monoclinic
Space group	$P2_1/n$
a / Å	7.660(3)
b / Å	23.988(10)
c / Å	9.385(4)
β / º	110.574(8)
Volume / Å^3	1614.6(11)
Z	4
μ(Mo Kα) / mm^{-1}	4.833
Crystal type	Colourless needle
Crystal size / mm	0.060×0.040×0.020
θ range (°)	3.82-18.77
Index ranges	$-6 \le h \le 6$ $-21 \le k \le 21$ $-8 \le l \le 7$
Collected Reflections	5580
Independent Reflections	980 (R_{int} = 0.1563)
Completeness to θ=18.77	78.1%
Final R indices [I>2σ(I)]	$R1$ = 0.0915 $wR2$ = 0.2264
Final R indices (all data)	$R1$ = 0.1429 $wR2$ = 0.2617
Largest diff. peak and hole / eÅ^{-3}	3.334 and -1.828

[a] $R1 = \sum \| |F_o| - |F_c| \| / \sum |F_o|$

[b] $wR2 = \sqrt{\sum \left[w\left(F_o^2 - F_c^2\right)^2 \right] / \sum \left[w\left(F_o^2\right)^2 \right]}$

[c] $w = 1/\left[\sigma^2\left(F_o^2\right) + \left(mP\right)^2 + nP \right]$ where $P = \left(F_o^2 + 2F_c^2\right)/3$

Table S2. Selected bond lengths (in Å) and angles (in degrees) for the Tb^{3+} coordination environment presented in [Tb(L)(HL)] (**1Tb_dry**).

Tb1–O10^{i}	2.17(3)	Tb1–O7^{iii}	2.24(4)
Tb1–O6	2.18(4)	Tb1–O9^{iv}	2.30(4)
Tb1–O3^{ii}	2.22(3)	Tb1–O2^{v}	2.33(4)
O10^{i} –Tb1–O6	168.5(13)	O3^{ii} –Tb1–O9^{iv}	96.8(13)
O10^{i} –Tb1–O3^{ii}	89.2(12)	O7^{iii} –Tb1–O9^{iv}	90.3(14)
O6–Tb1–O3^{ii}	79.4(13)	O10^{i} –Tb1–O2^{v}	93.1(13)
O10^{i} –Tb1–O7^{iii}	92.6(13)	O6–Tb1–O2^{v}	89.4(14)
O6–Tb1–O7^{iii}	98.8(15)	O3^{ii} –Tb1–O2^{v}	93.5(13)
O3^{ii} –Tb1–O7^{iii}	172.2(15)	O7^{iii} –Tb1–O2^{v}	78.9(15)
O10^{i} –Tb1–O9^{iv}	99.6(13)	O9^{iv} –Tb1–O2^{v}	163.7(10)
O6–Tb1–O9^{iv}	80.1(15)		

[a] Symmetry transformations used to generate equivalent atoms: (i) *x*+1/2, -*y*+1/2, *z*-1/2; (ii) *x*+1/2, -*y*+1/2, *z*+1/2; (iii) *x*+1, *y*, *z*; (iv) *x*, *y*, *z*-1; (v) *x*+1, *y*, *z*+1.

Table S3. Hydrogen bonding geometry (distances in Å and angles in degrees) of [Tb(L)(HL)] (**1Tb_dry**).

D-H···A	d(D···A)	<(DHA)
O8–H8A···O5^{vi}	3.32(4)	155

[a] Symmetry transformation used to generate equivalent atoms: (vi) -*x*+2, -*y*+1, -*z*+1.

2. NMR characterization

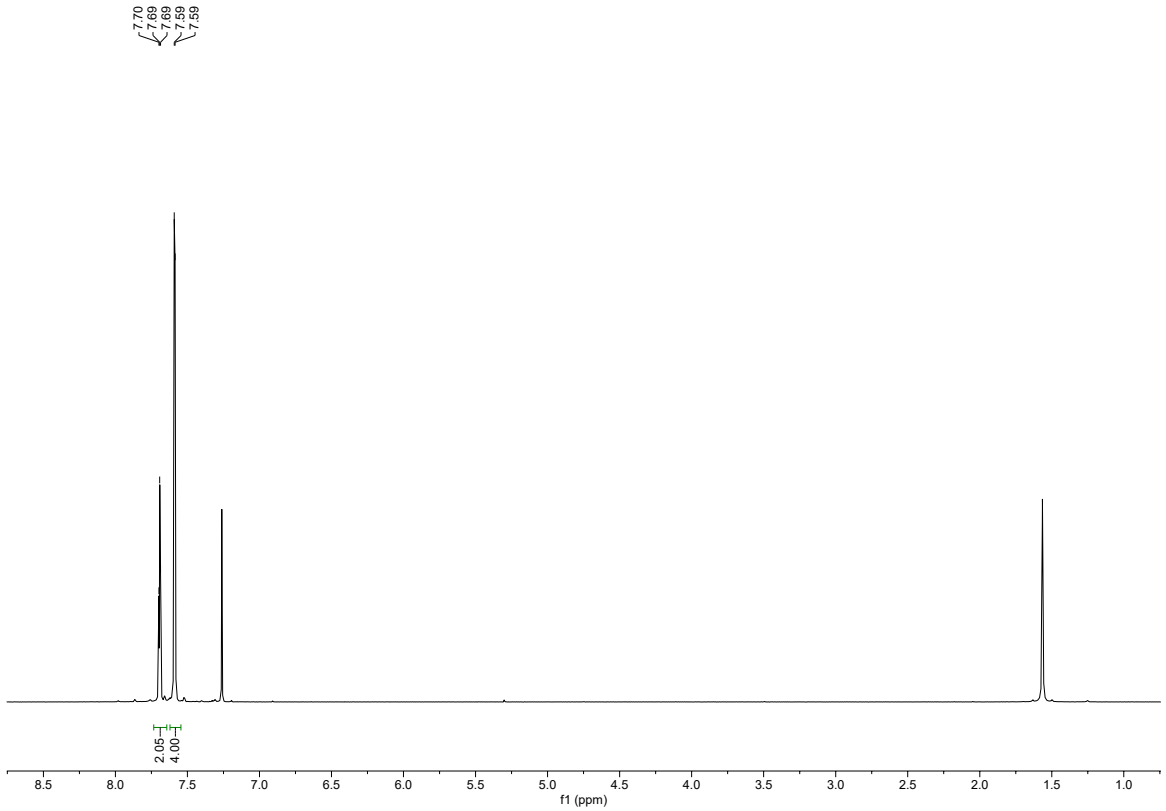

Fig. S1 ^{1}H-NMR spectrum of 3,3′,5,5′-tetrabromo-1,10-biphenyl in $CDCl_3$.

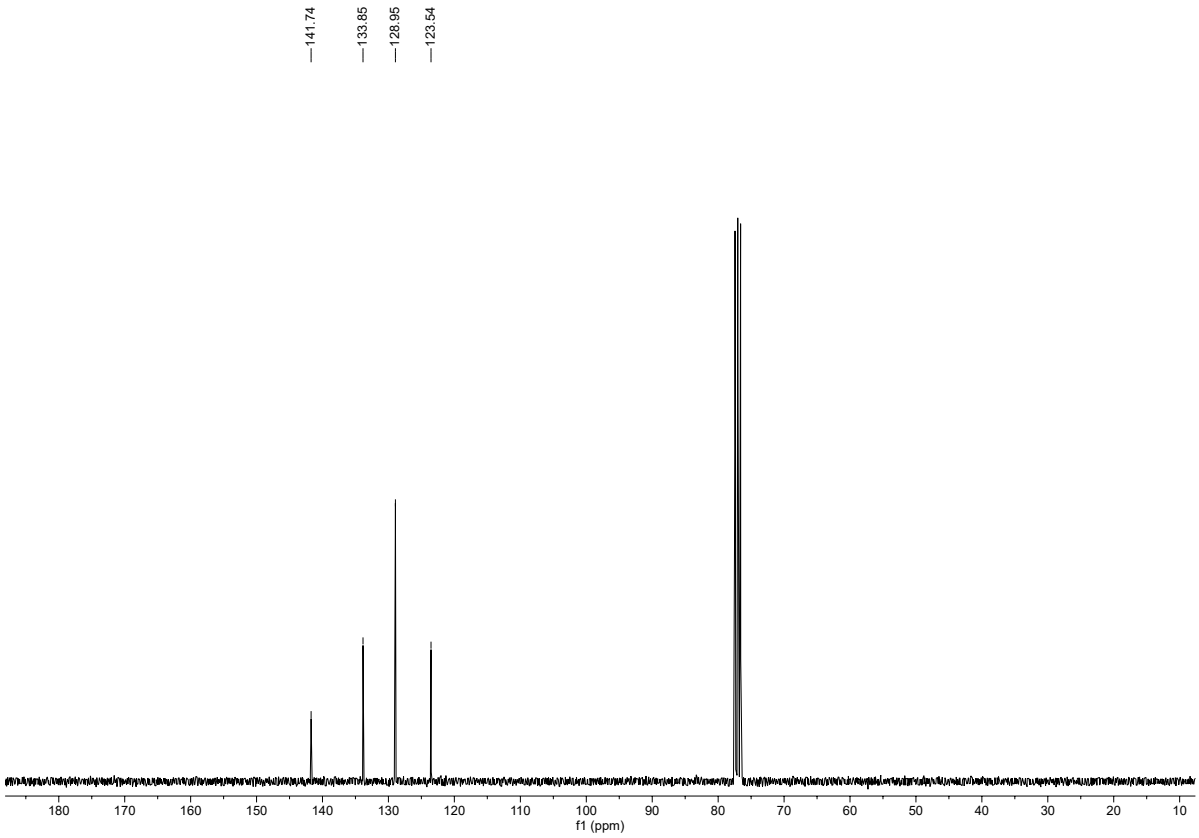

Fig. S2 ^{13}C-NMR spectrum of 3,3′,5,5′-tetrabromo-1,10-biphenyl in $CDCl_3$.

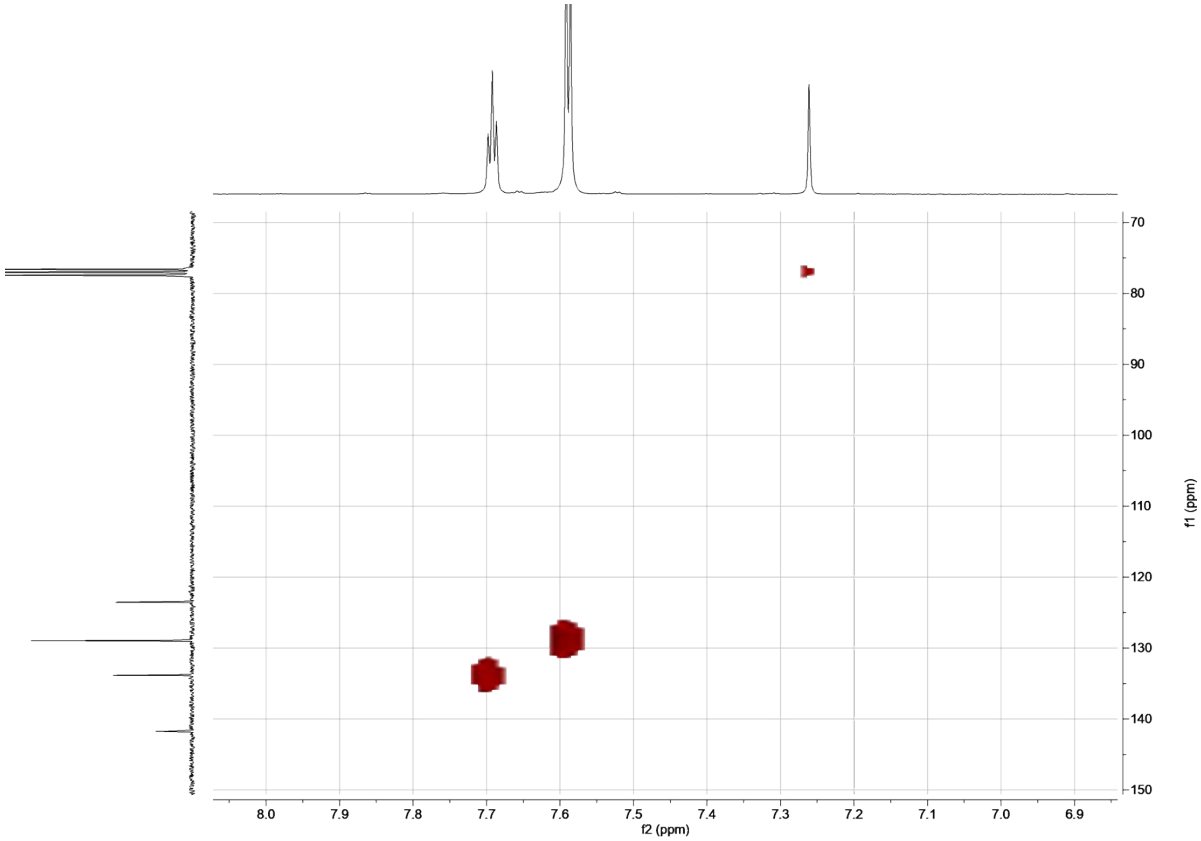

Fig S3. HSQC spectrum of 3,3′,5,5′-tetrabromo-1,10-biphenyl in $CDCl_3$.

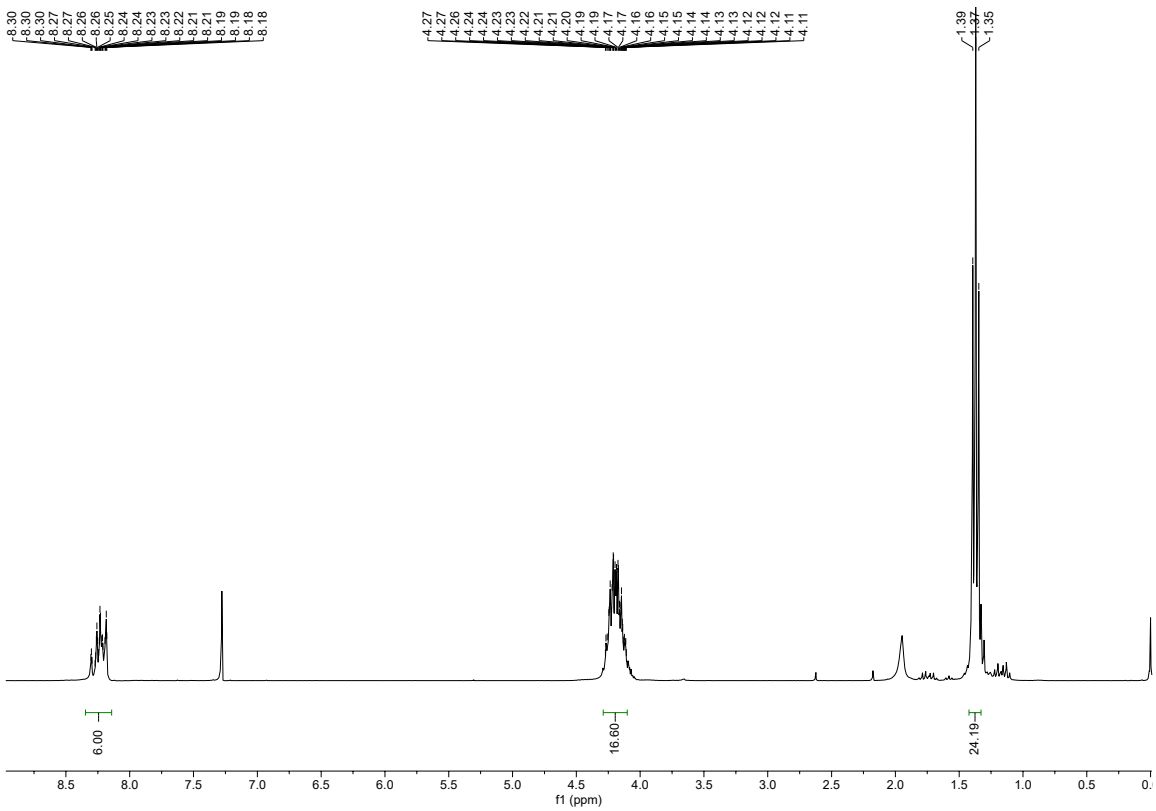

Fig. S4 ^{1}H-NMR spectrum of octaethyl-[1,10-biphenyl]-3,3′,5,5′-tetrayltetrakis(phosphonate) in $CDCl_3$.

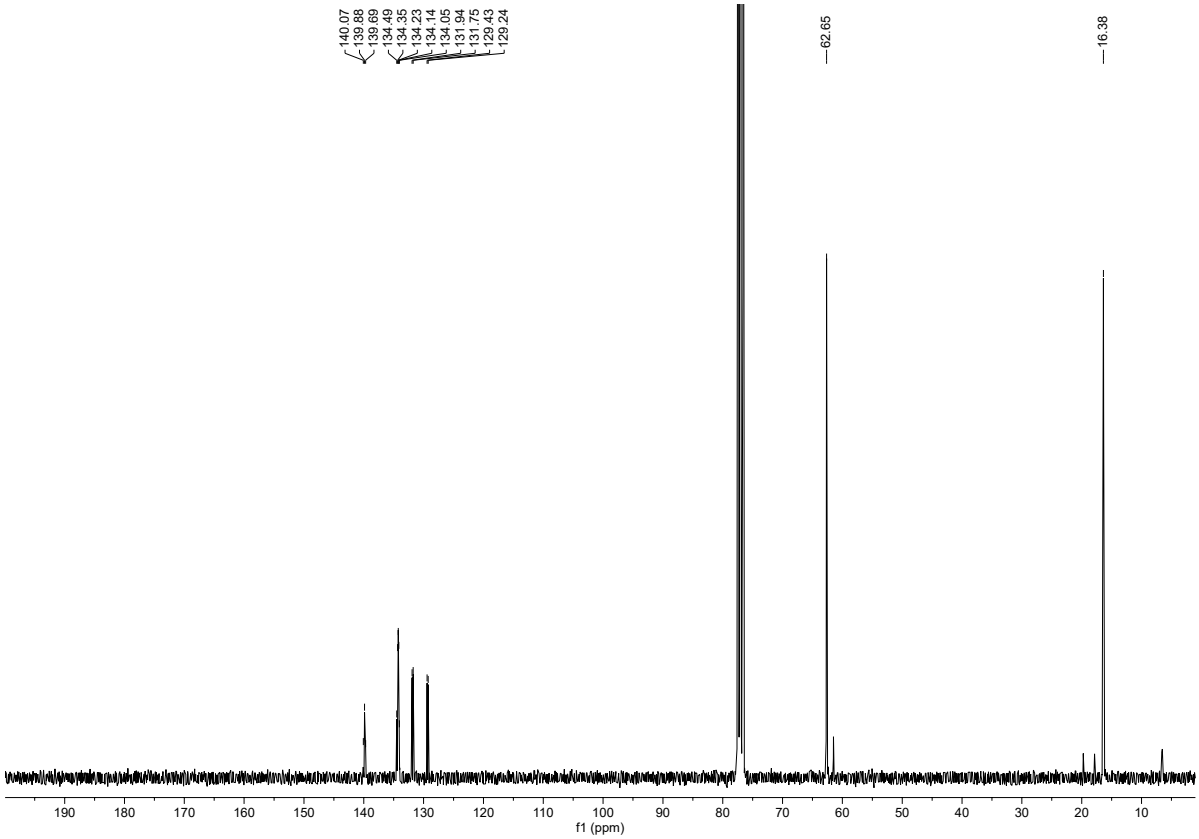

Fig. S5 ^{13}C-NMR spectrum of octaethyl-[1,10-biphenyl]-3,3′,5,5′-tetrayltetrakis(phosphonate) in $CDCl_3$.

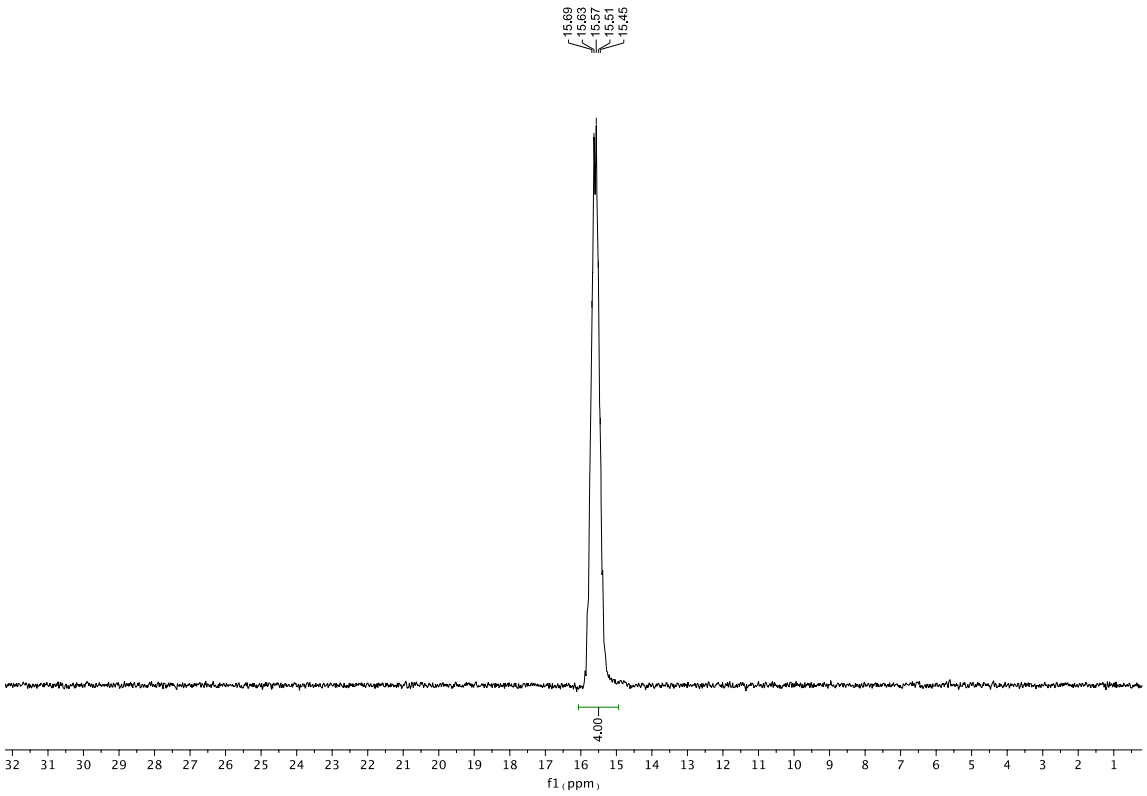

Fig. S6 ^{31}P-NMR spectrum of octaethyl-[1,10-biphenyl]-3,3′,5,5′-tetrayltetrakis(phosphonate) in $CDCl_3$.

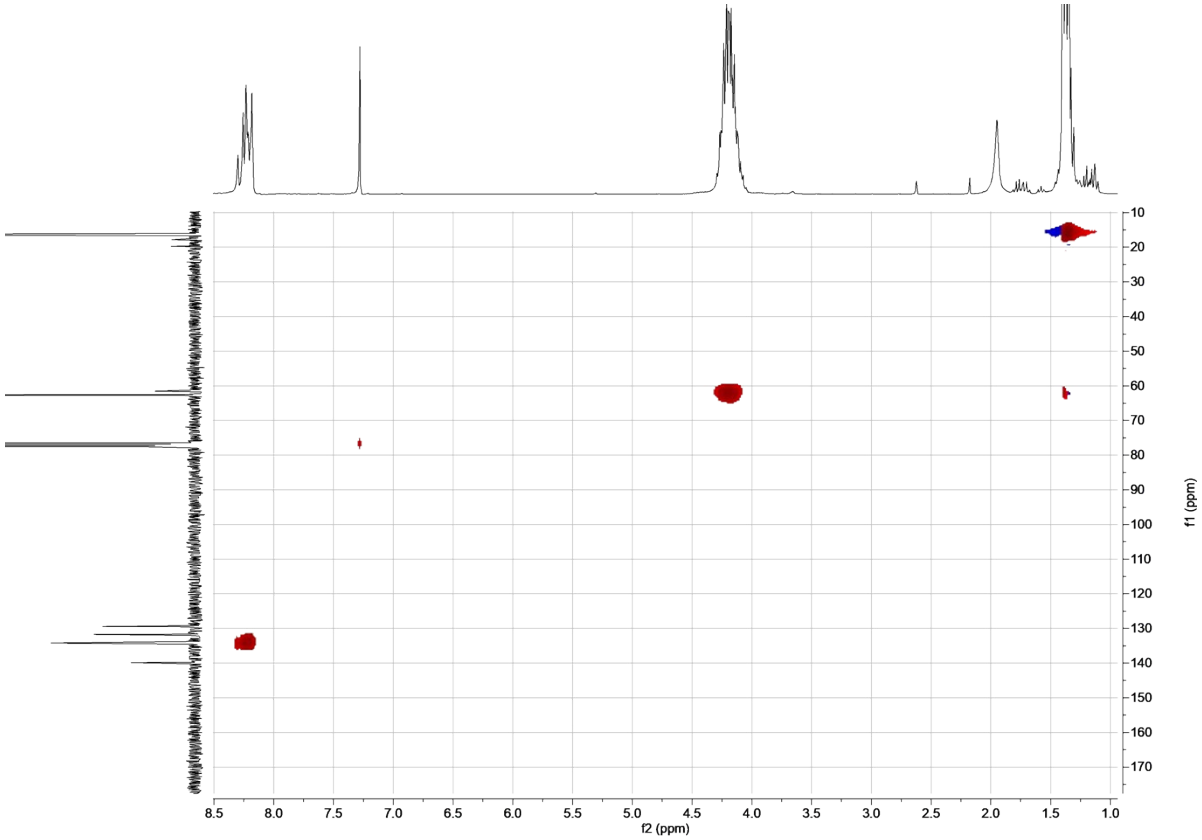

Fig. S7 HSQC spectrum of octaethyl-[1,10-biphenyl]-3,3′,5,5′-tetrayltetrakis(phosphonate) in $CDCl_3$.

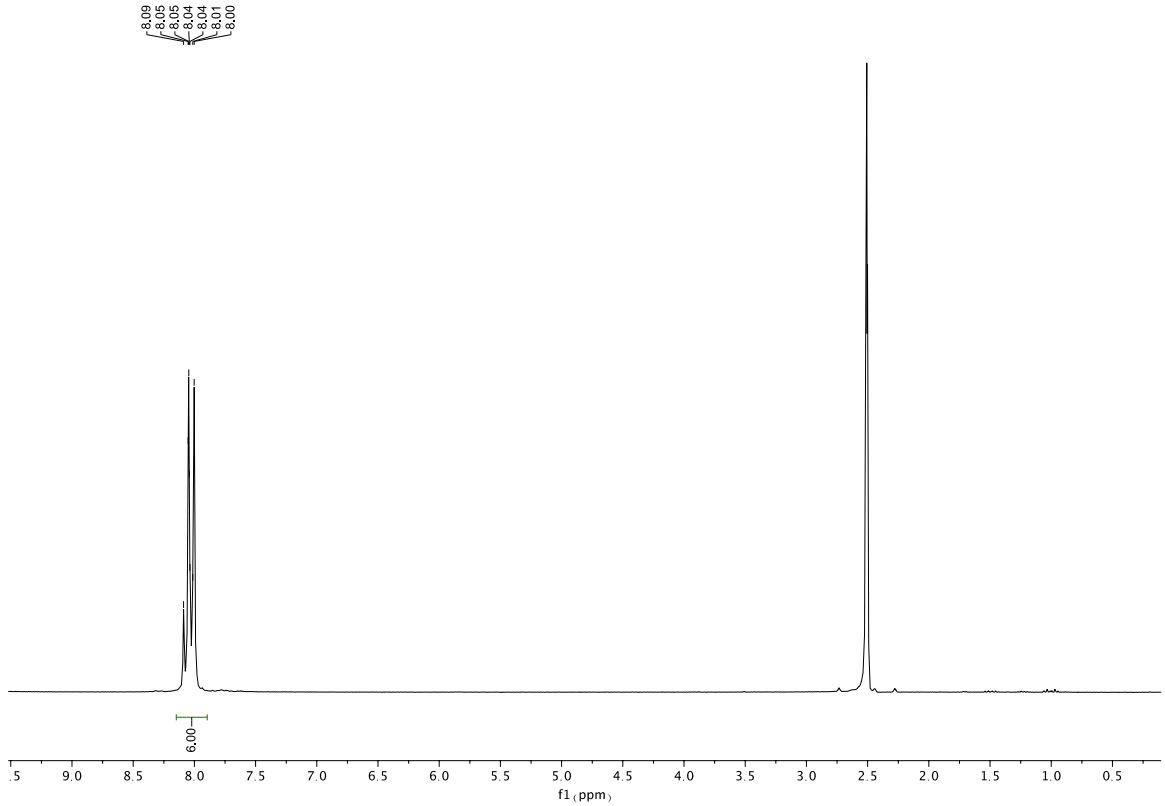

Fig. S8 ^{1}H-NMR spectrum of [1,1-biphenyl]-3,3′,5,5′-tetrayltetrakis(phosphonic acid) (H_8btp) in DMSO-d_6.

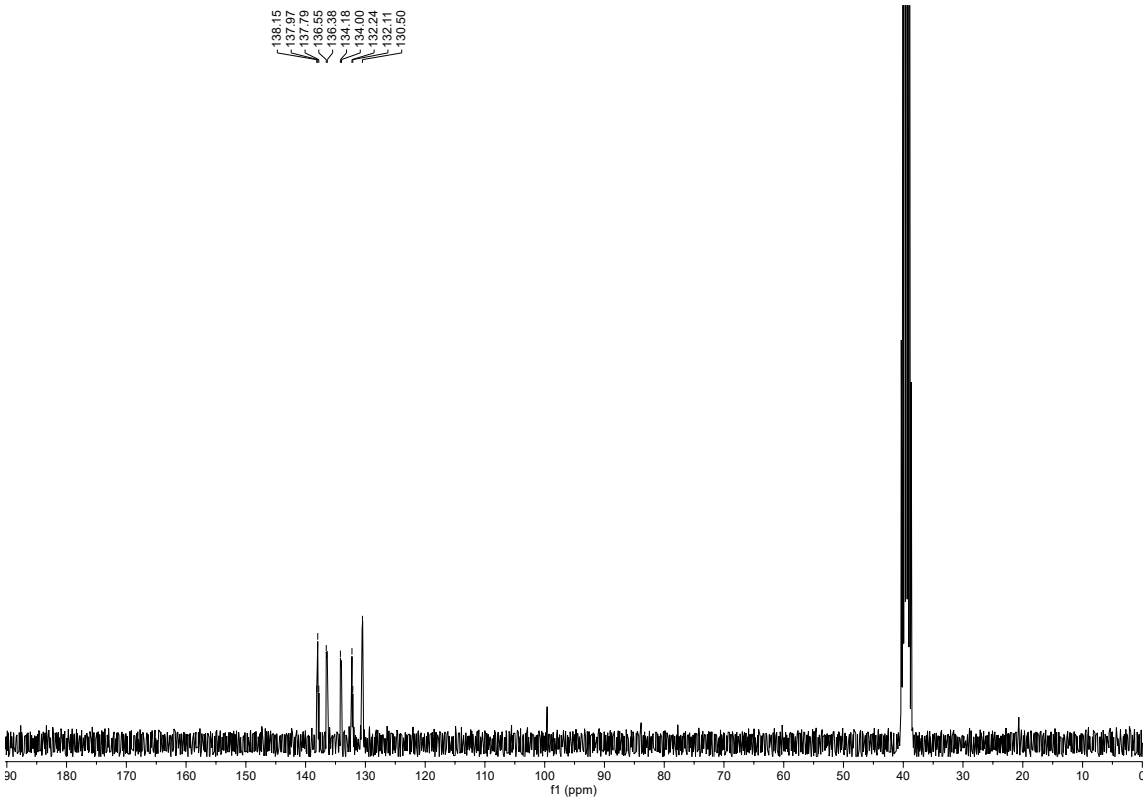

Fig. S9 ^{13}C-NMR spectrum of [1,1-biphenyl]-3,3′,5,5′-tetrayltetrakis(phosphonic acid) (H_8btp) in DMSO-d_6.

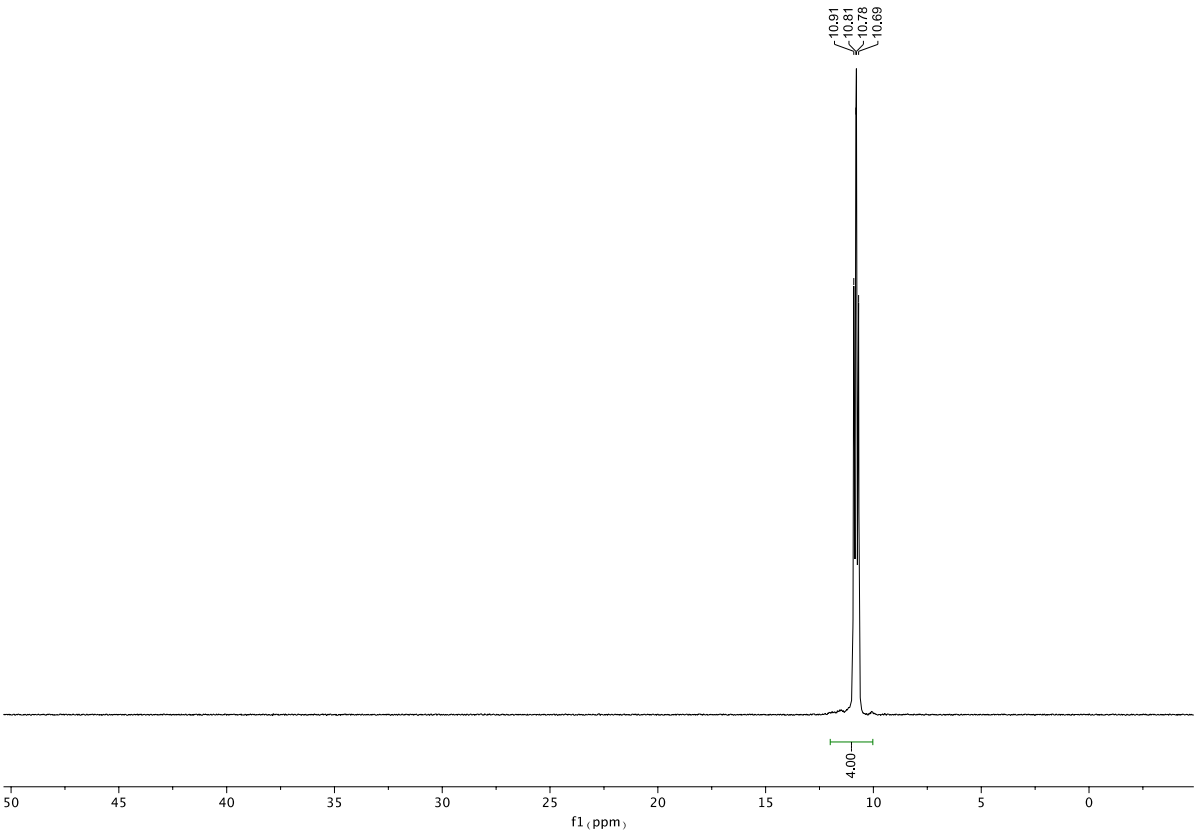

Fig. S10 ^{31}P-NMR spectrum of [1,1-biphenyl]-3,3′,5,5′-tetrayltetrakis(phosphonic acid) (H_8btp) in DMSO-d_6.

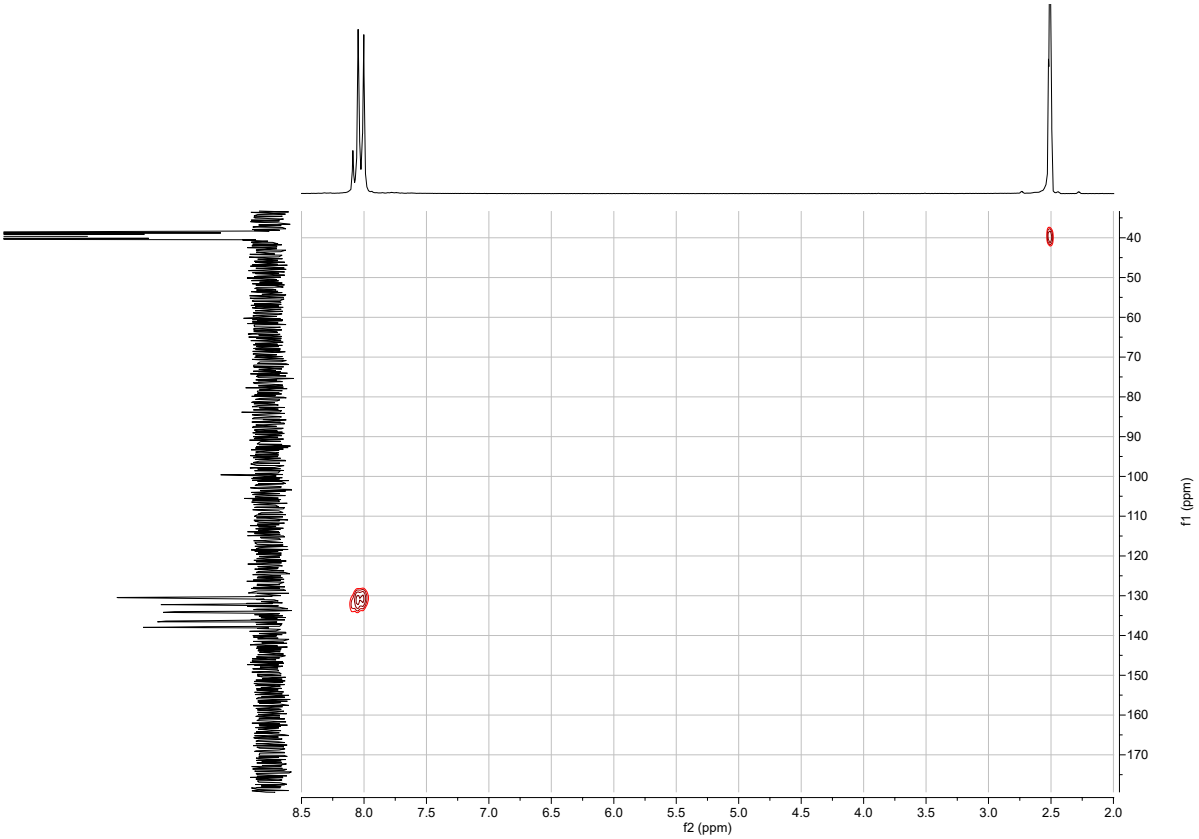

Fig. S11 HSQC spectrum of [1,1-biphenyl]-3,3′,5,5′-tetrayltetrakis(phosphonic acid) (H_8btp) in DMSO-d_6.

3. Crystallographic Studies

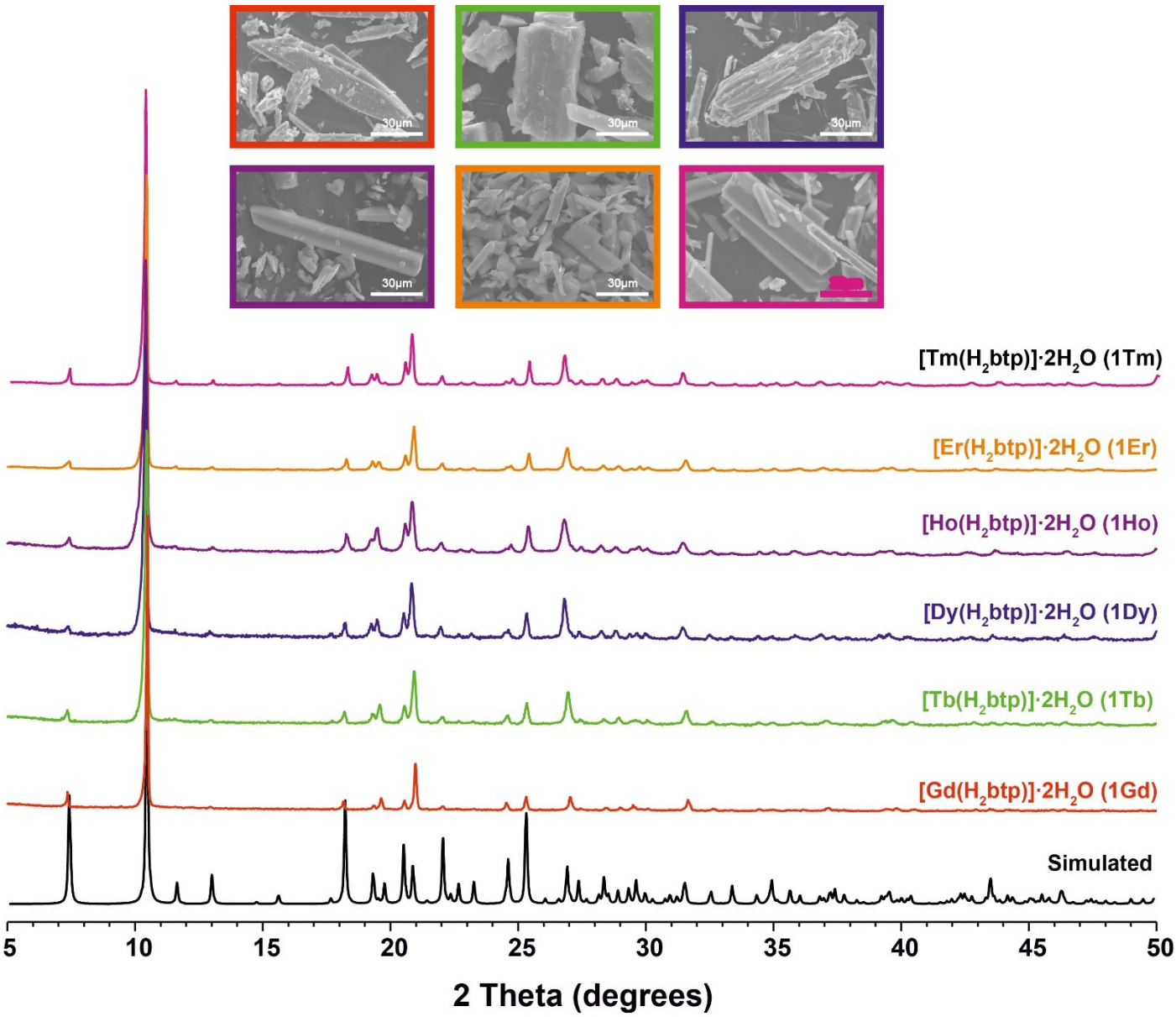

Fig. S12 Powder X-ray diffraction studies and SEM images of the series of materials were formulated as [Ln(H_5btp)]·2H_2O [where Ln^{3+} = Gd^{3+} (**1Gd**), Tb^{3+} (**1Tb**), Dy^{3+} (**1Dy**), Ho^{3+} (**1Ho**), Er^{3+} (**1Er**), and Tm^{3+} (**1Tm**)].

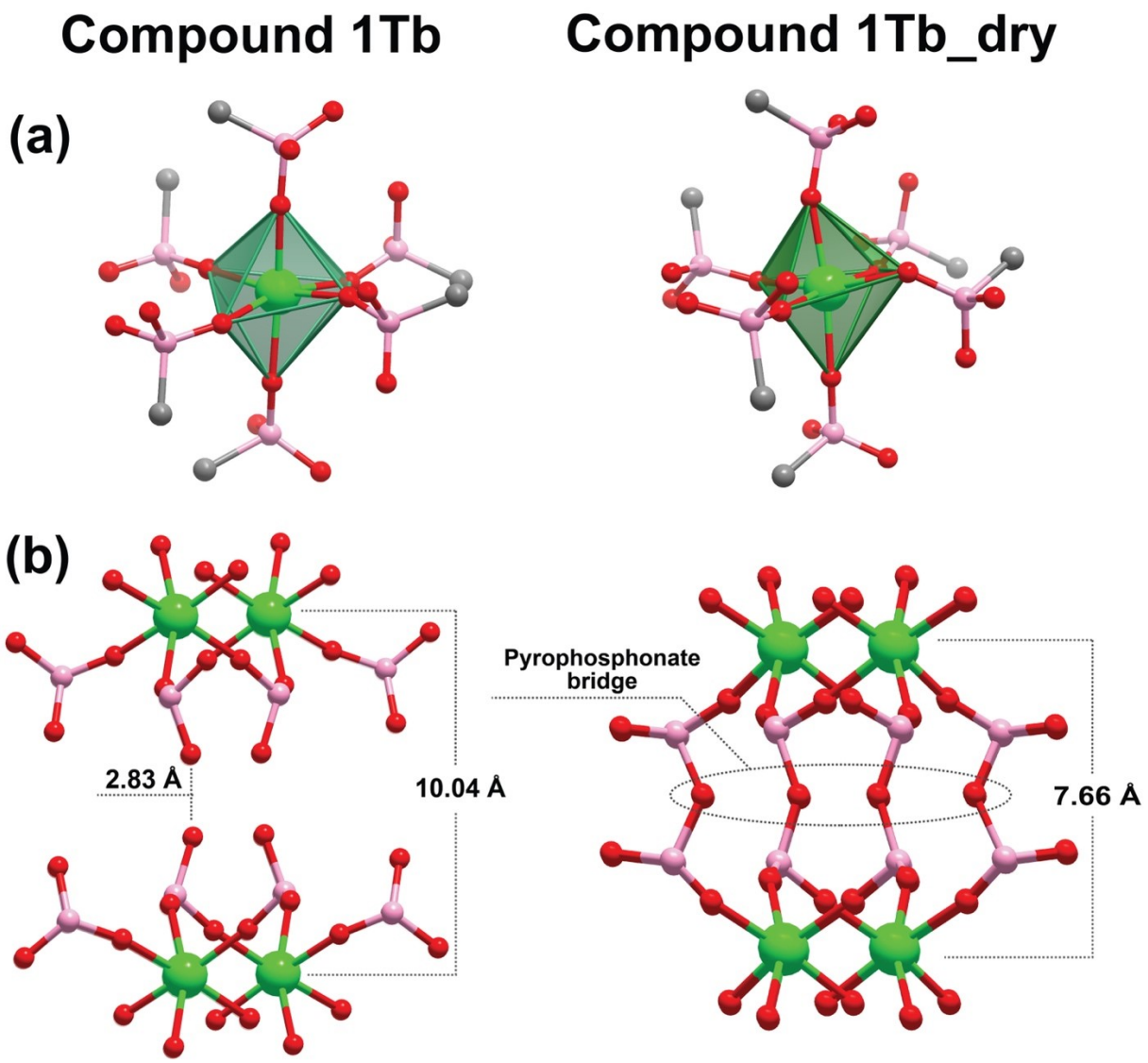

Fig. S13 Coordination environment of the Tb^{3+} centre in $[Tb(H_5btp)]\cdot 2H_2O$ (**1Tb**)[11] and [Tb(L)(HL)] (**1Tb_dry**). (**b**) Schematic representation of the decrease in the average Tb···Tb distances during the single-crystal-to-single-crystal transformation as well as the formation of the pyrophosphonate bridges.

4. Electron Microscopy Studies: EDS Mapping

EDS mapping studies reveal a uniform distribution of the heaviest elements among the bulk [Ln(H_5btp)]·2H_2O materials [where Ln^{3+} = Gd^{3+} (**1Gd**), Tb^{3+} (**1Tb**), Dy^{3+} (**1Dy**), Ho^{3+} (**1Ho**), Er^{3+} (**1Er**) and Tm^{3+} (**1Tm**)], ultimately evidencing the presence of pure phases, as further corroborated by the powder X-ray diffraction studies (Figure S11).

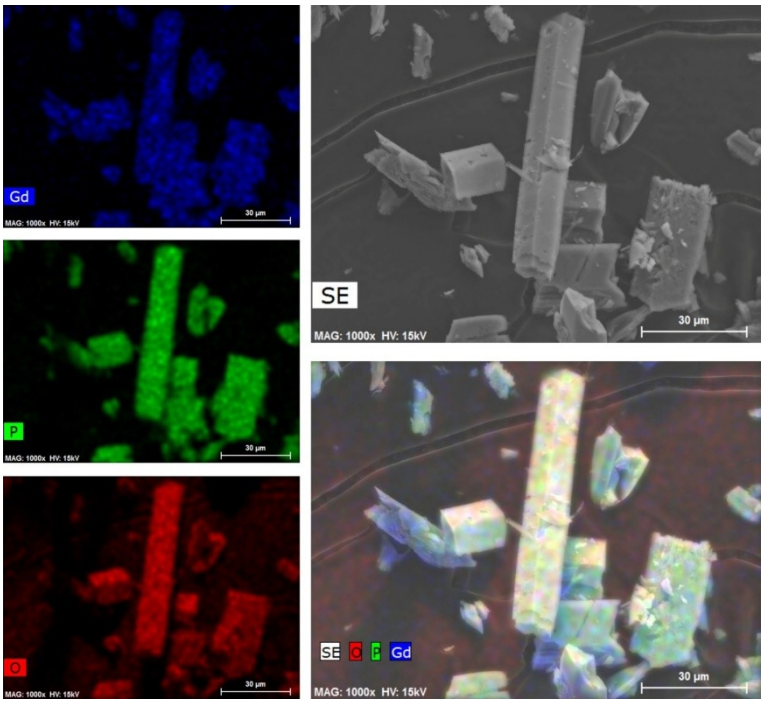

Fig. S14 EDS mapping of a representative portion of [Gd(H_5btp)]·2H_2O (**1Gd**) bulk material. Gd : P ratio of 1.0 : 3.6.

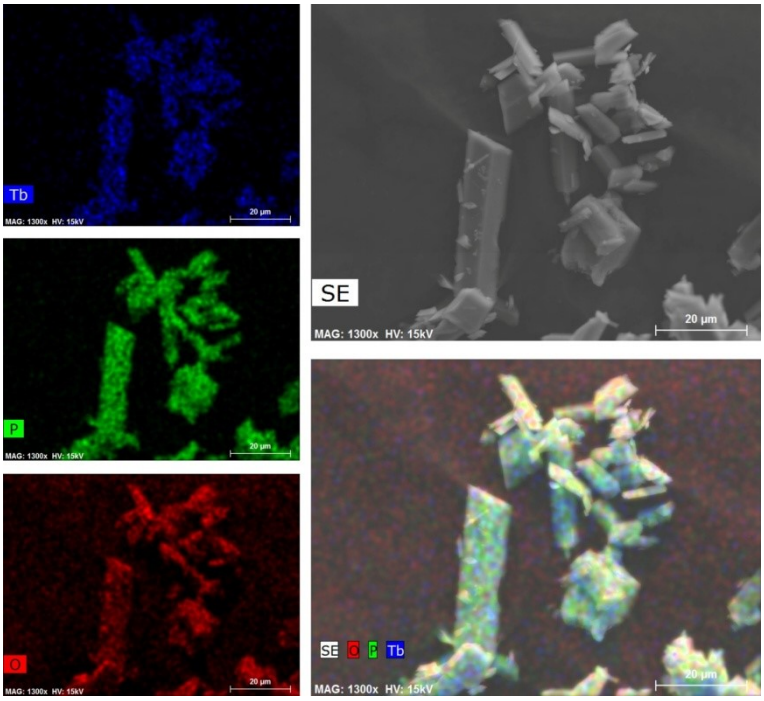

Fig. S15 EDS mapping of a representative portion of [Tb(H_5btp)]·2H_2O (**1Tb**) bulk material. Tb : P ratio of 1.0 : 3.6.

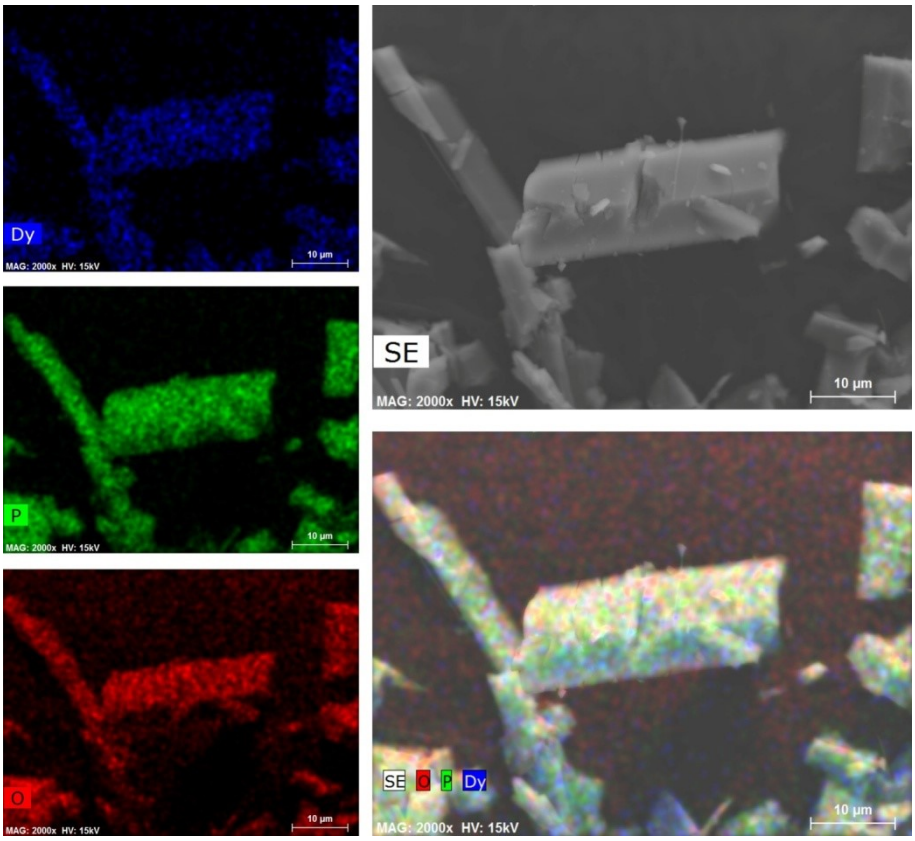

Fig. S16 EDS mapping of a representative portion of [Dy(H_5btp)]·2H_2O (**1Dy**) bulk material. Dy : P ratio of 1.0 : 3.7.

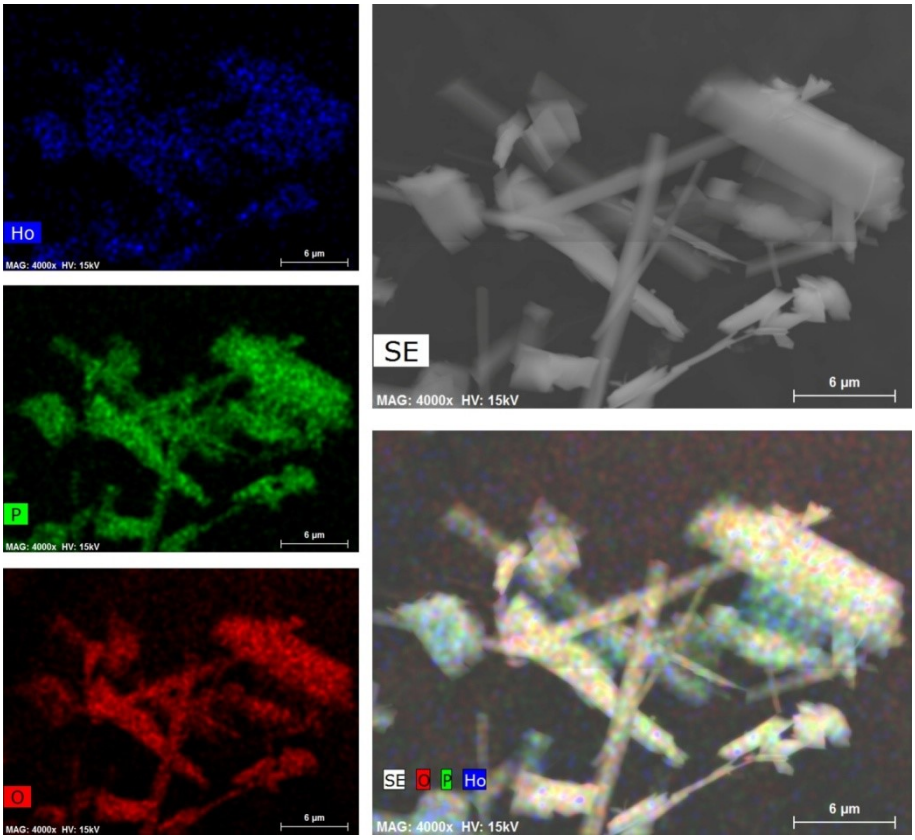

Fig. S17 EDS mapping of a representative portion of [Ho(H_5btp)]·2H_2O (**1Ho**) bulk material. Ho : P ratio of 1.0 : 3.7.

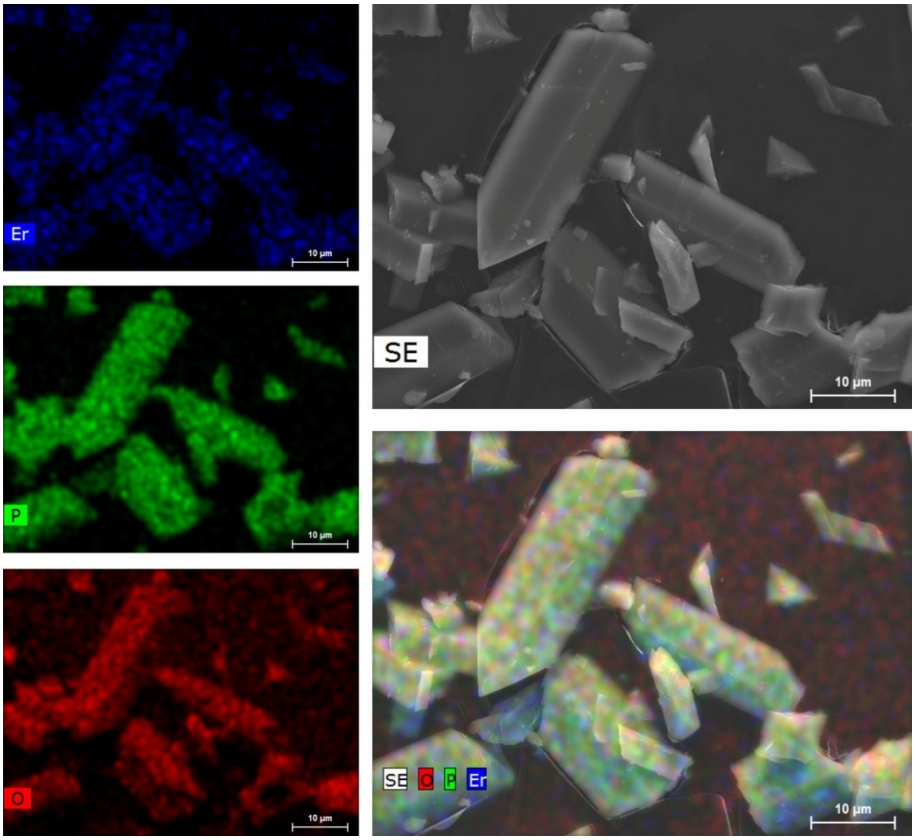

Fig. S18 EDS mapping of a representative portion of [Er(H_5btp)]·2H_2O (**1Er**) bulk material. Er : P ratio of 1.0 : 3.6.

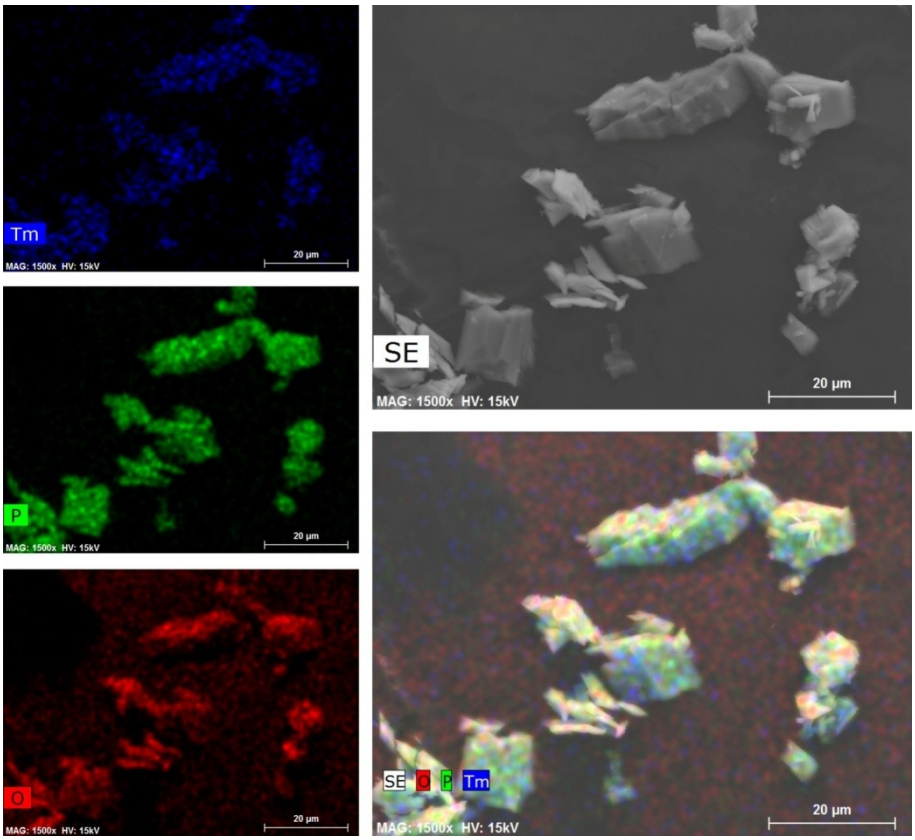

Fig. S19 EDS mapping of a representative portion of [Tm(H_5btp)]·2H_2O (**1Tm**) bulk material. Tm : P ratio of 1.0 : 3.7.

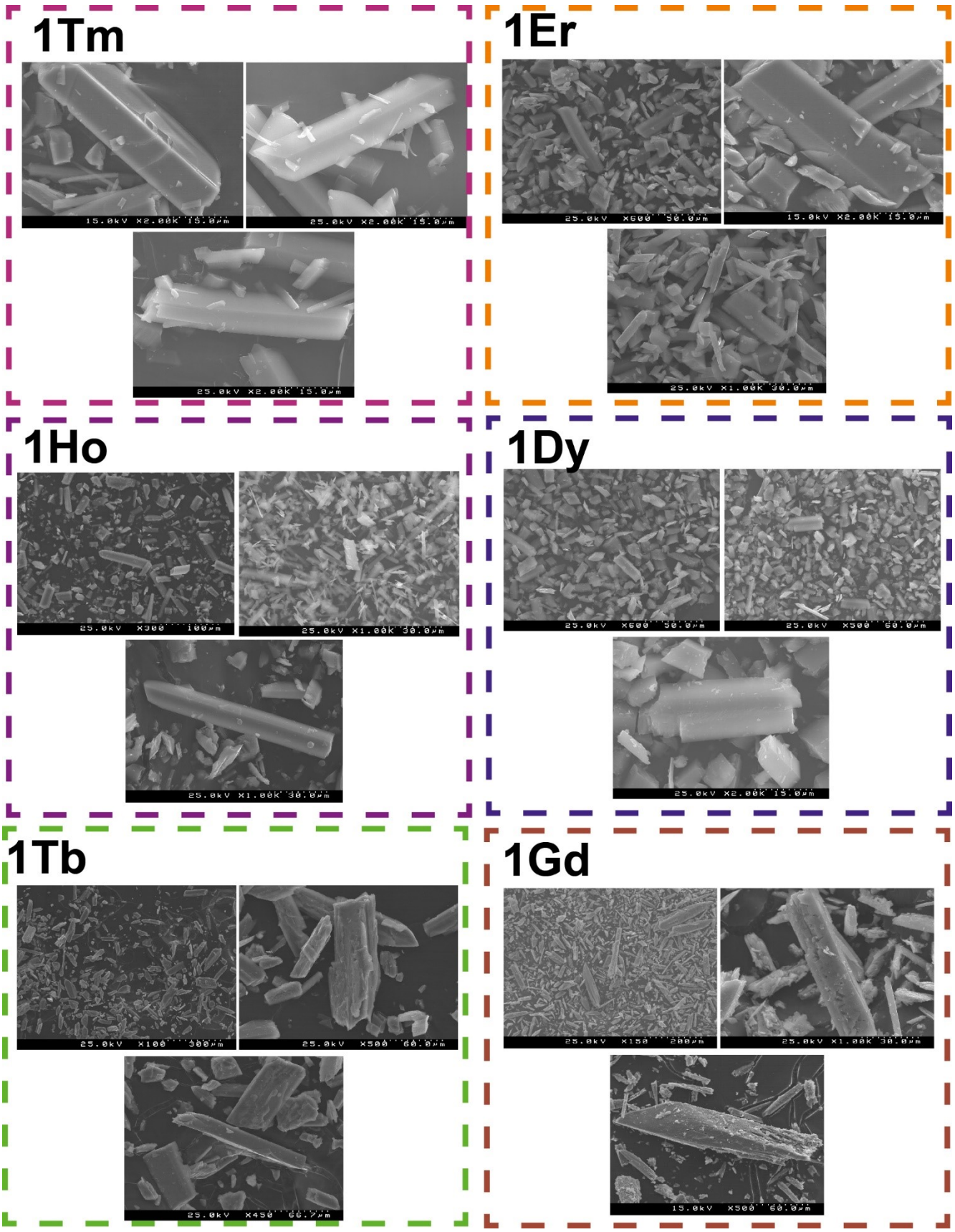

Fig. S20. SEM images at different magnifications of the $[Ln(H_5btp)]\cdot 2H_2O$ materials [$Ln^{3+} = Gd^{3+}$ (**1Gd**), Tb^{3+} (**1Tb**), Dy^{3+} (**1Dy**), Ho^{3+} (**1Ho**), Er^{3+} (**1Er**), and Tm^{3+} (**1Tm**)].

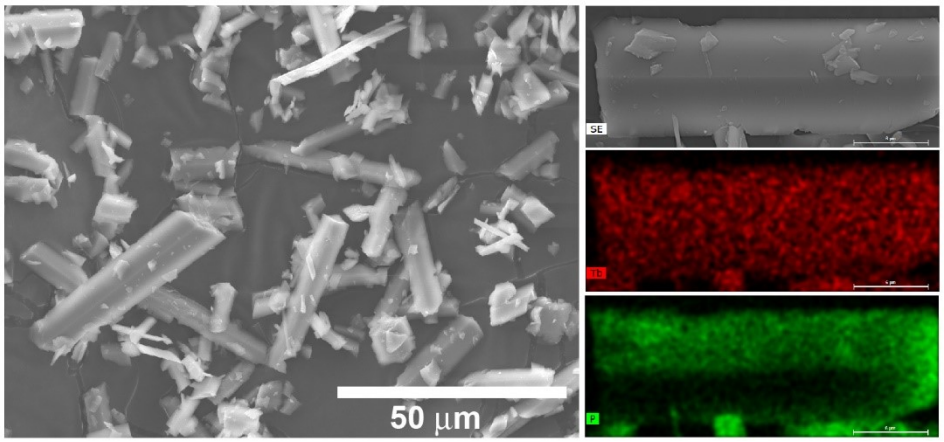

Fig. S21. SEM images and EDS mapping of Tb(L)(HL)] (**1Tb_dry**). Tb : P ratio of 1.0 : 3.6.

5. FT-IR spectroscopy

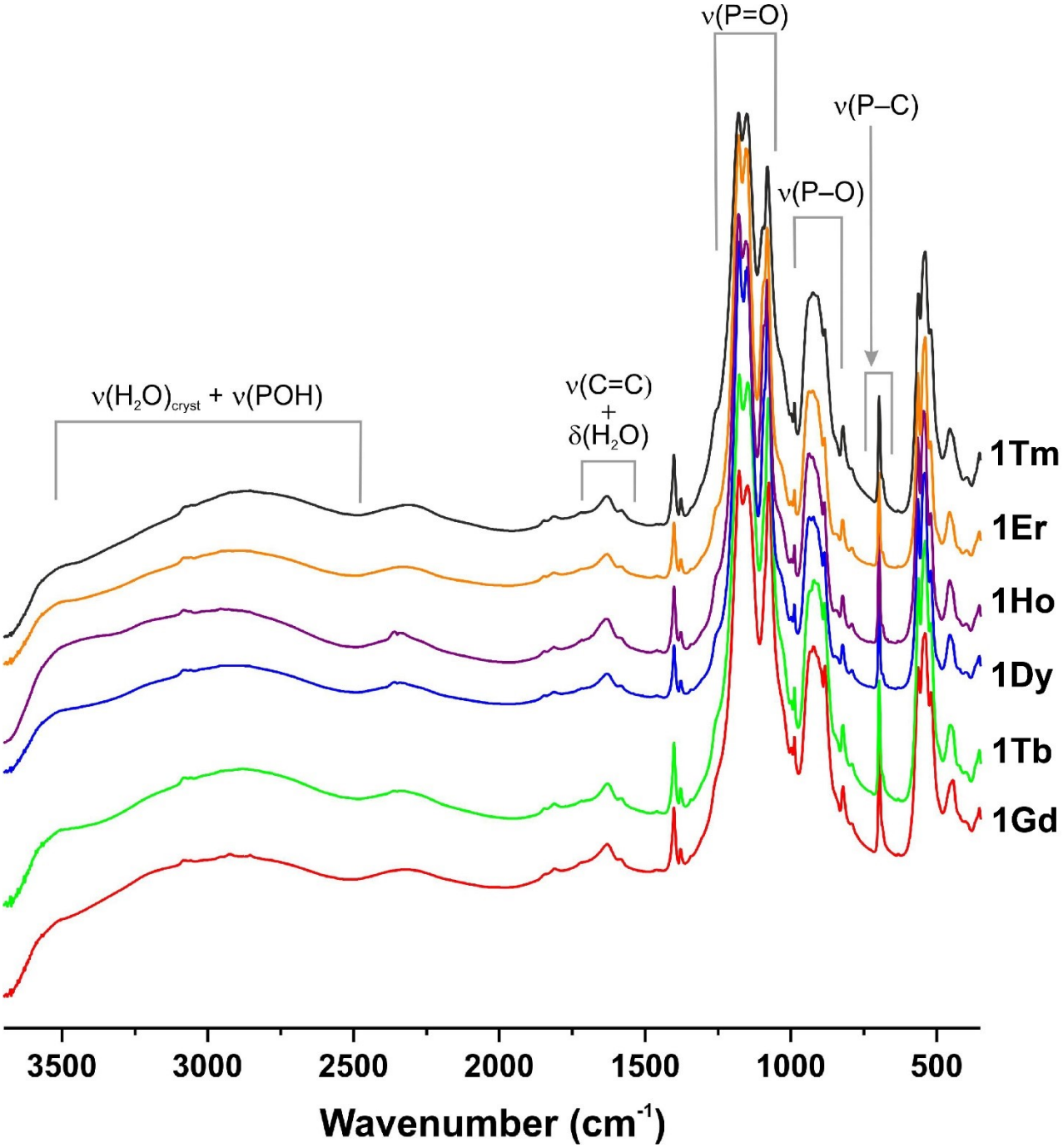

Fig. S22 FT-IR spectra of the isotypical series of $[Ln(H_5btp)]\cdot 2H_2O$ materials [Ln^{3+} = Gd^{3+} (**1Gd**), Tb^{3+} (**1Tb**), Dy^{3+} (**1Dy**), Ho^{3+} (**1Ho**), Er^{3+} (**1Er**), and Tm^{3+} (**1Tm**)].

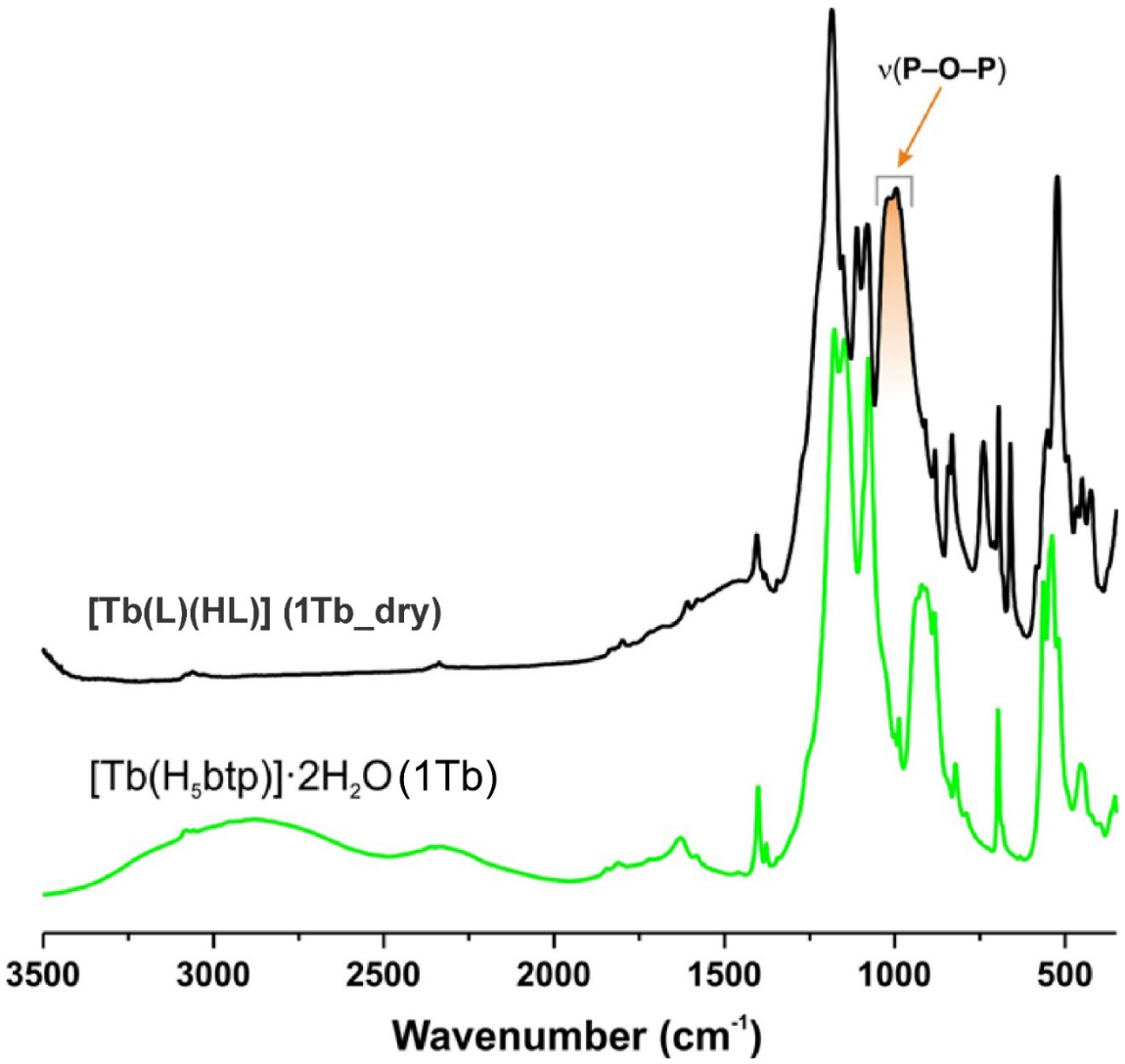

Fig. S23 Comparison between the FT-IR spectral features of $[Tb(H_5btp)]\cdot 2H_2O$ (**1Tb**) and [Tb(L)(HL)] (**1Tb_dry**).

6. Thermogravimetry and Thermodiffractometry

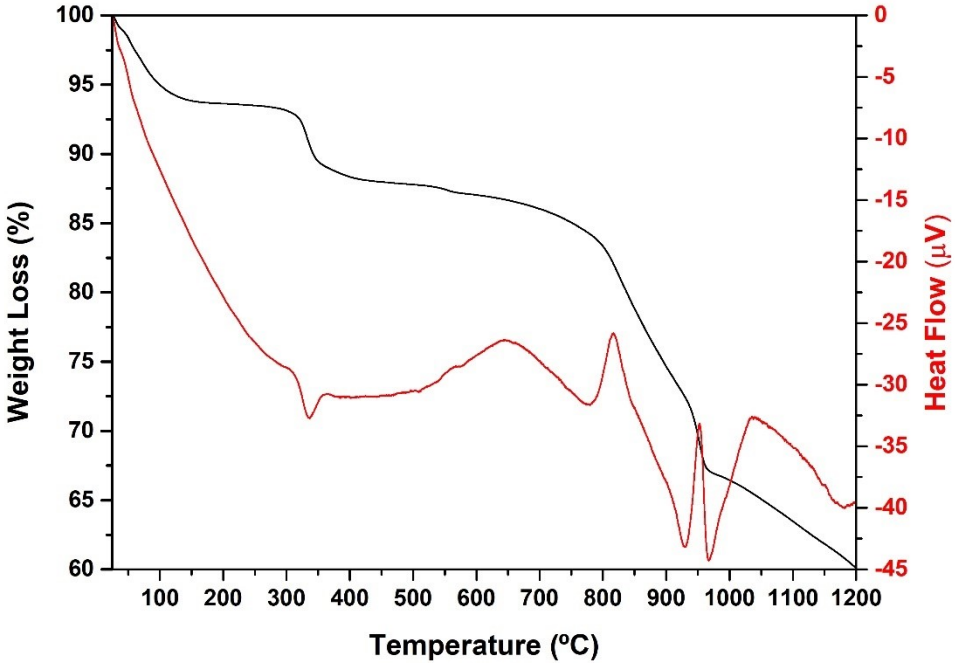

Fig. S24 Thermogram and DSC analysis of [Tb(H_5btp)]·2H_2O (**1Tb**) material collected between ambient temperature and *ca.* 1200 ºC.

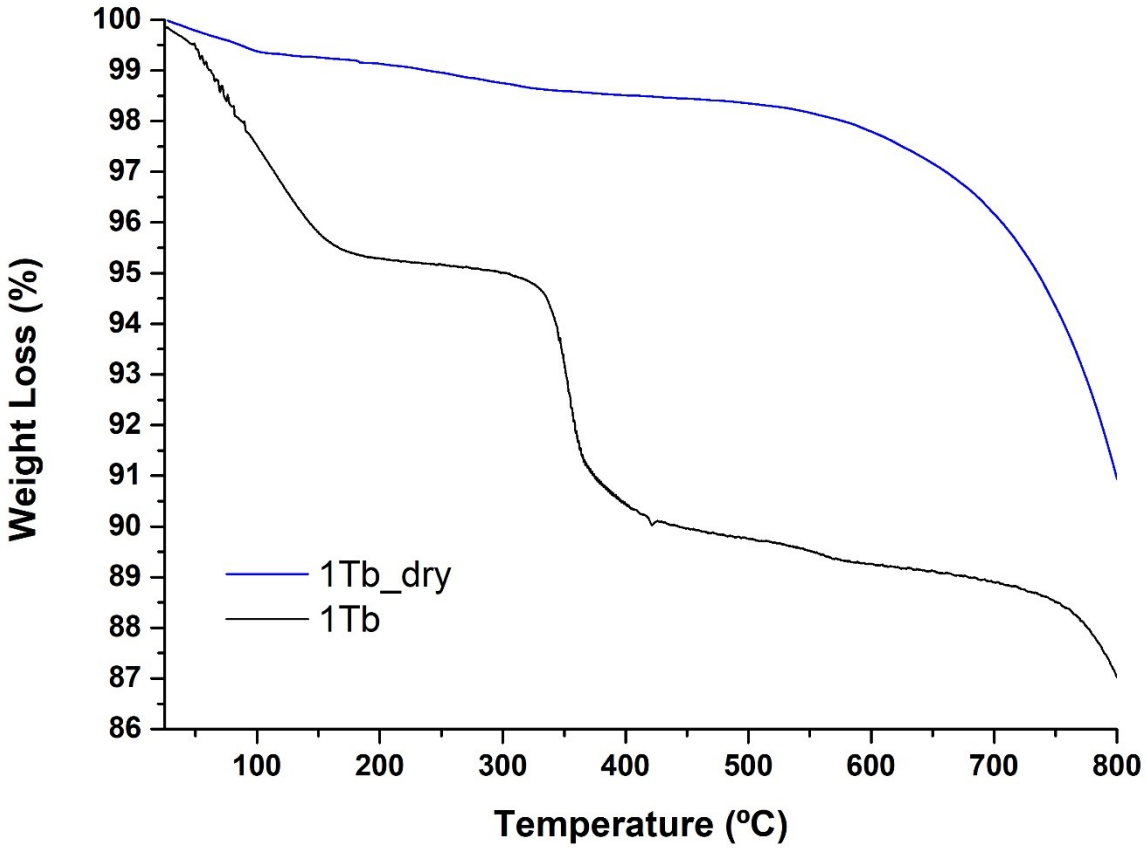

Fig. S25 Thermogram of [Tb(H_5btp)]·2H_2O (**1Tb**) compared with that of [Tb(L)(HL)] (**1Tb_dry**) collected between ambient temperature and *ca.* 800 ºC.

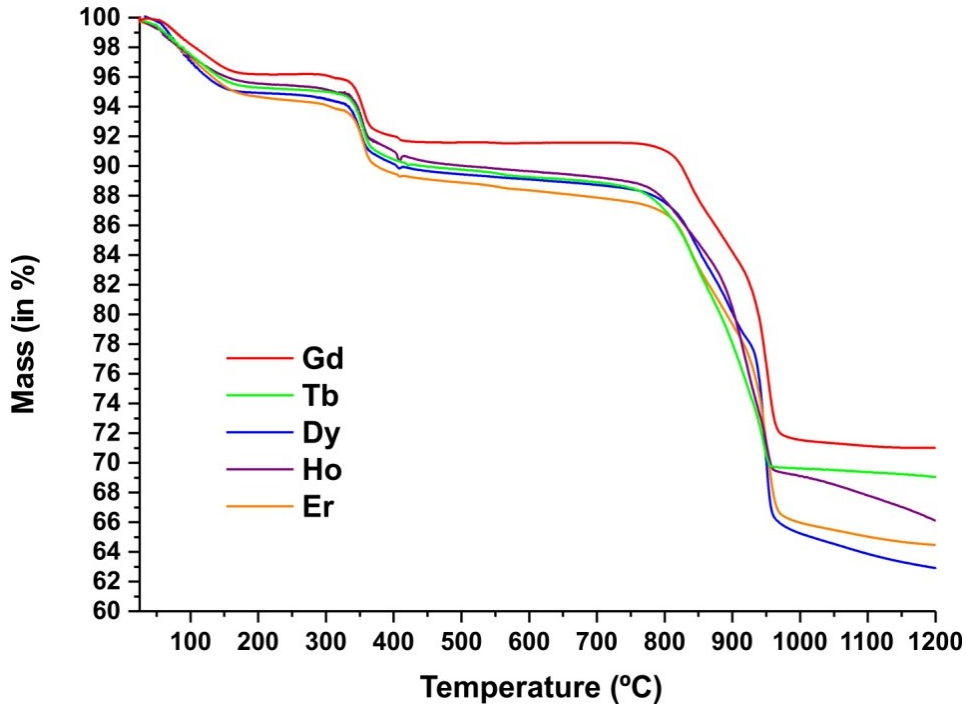

Fig. S26 Thermograms of the isotypical series of $[Ln(H_5btp)]\cdot 2H_2O$ materials [where Ln^{3+} = Gd^{3+} (**1Gd**), Tb^{3+} (**1Tb**), Dy^{3+} (**1Dy**), Ho^{3+} (**1Ho**), Er^{3+} (**1Er**) and Tm^{3+} (**1Tm**)] collected between ambient temperature and *ca.* 1200 ºC.

Table S4. Temperature range, weight loss and assignment of the released component attributed to the weight loss for $[Tb(H_5btp)]\cdot 2H_2O$ (**1Tb**) material.

Temperature (ºC)	Weight Loss (%)	Component released
Amb. Temp. - 250	4.83	Two crystallization water molecules
250-650	6.05	Two water molecules from the pyrophosphonate formation
650-1200	20.12	Decomposition of the organic matter

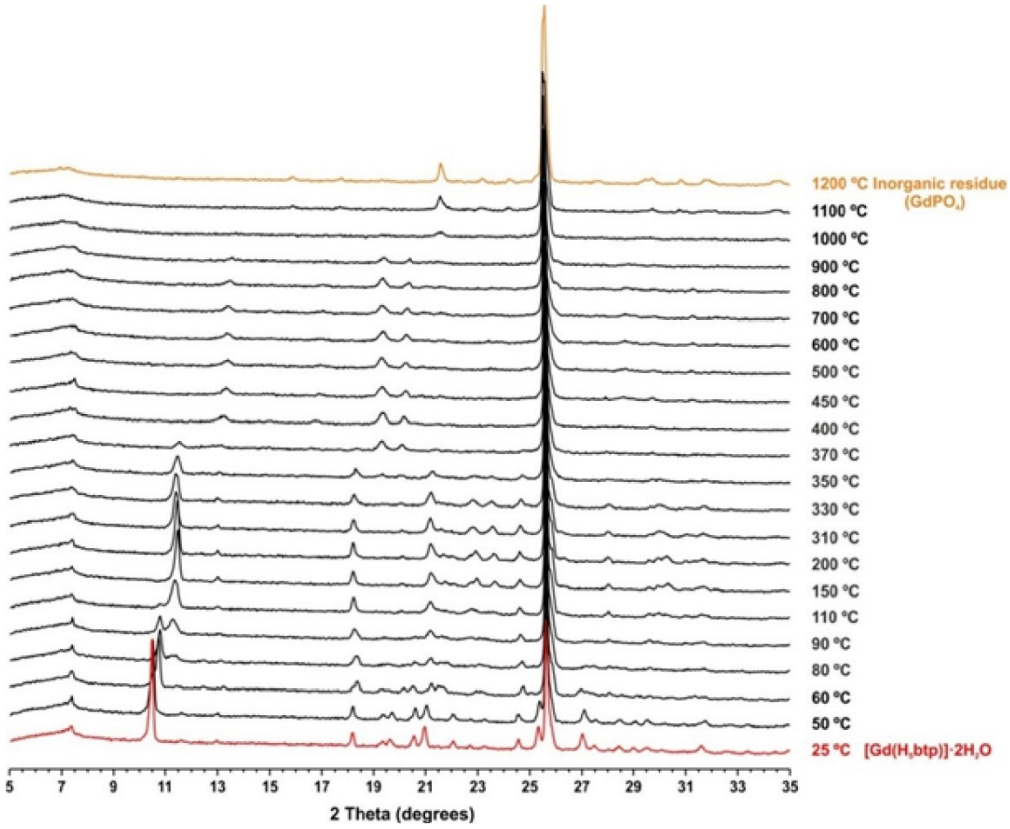

Fig. S27 VTPXRD studies of $[Gd(H_5btp)]\cdot 2H_2O$ (**1Gd**) collected between ambient temperature and *ca.* 1200 ºC.

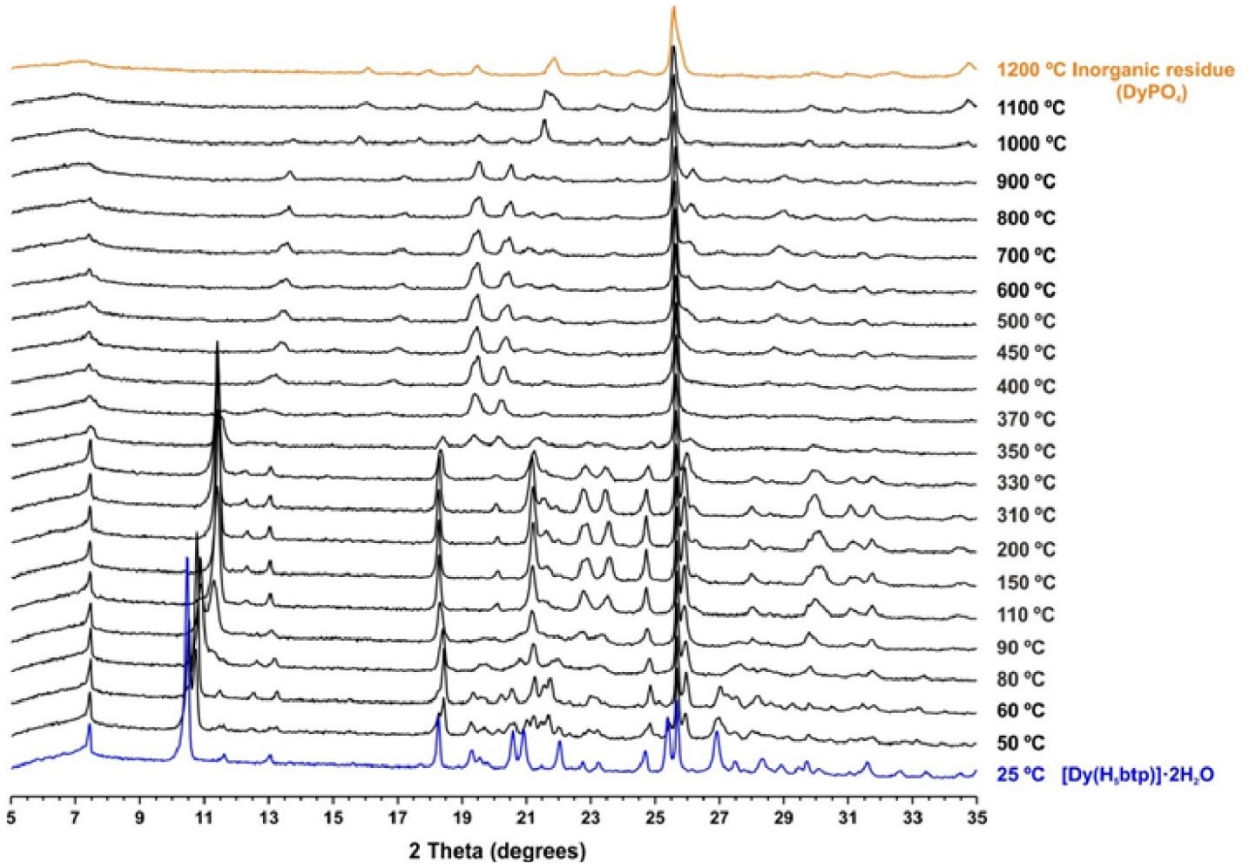

Fig. S28 VTPXRD studies of $[Dy(H_5btp)]\cdot 2H_2O$ (**1Dy**) collected between ambient temperature and *ca.* 1200 ºC.

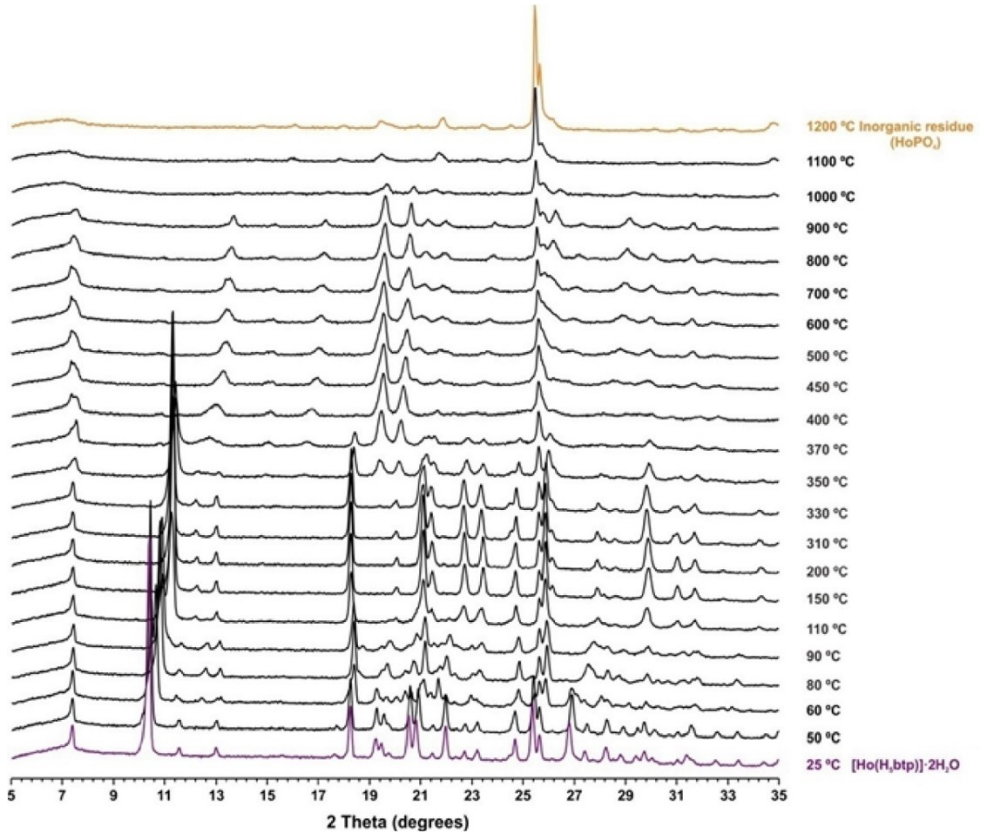

Fig. S29 VTPXRD studies of [Ho(H_5btp)]·2H_2O (**1Ho**) collected between ambient temperature and *ca.* 1200 ºC.

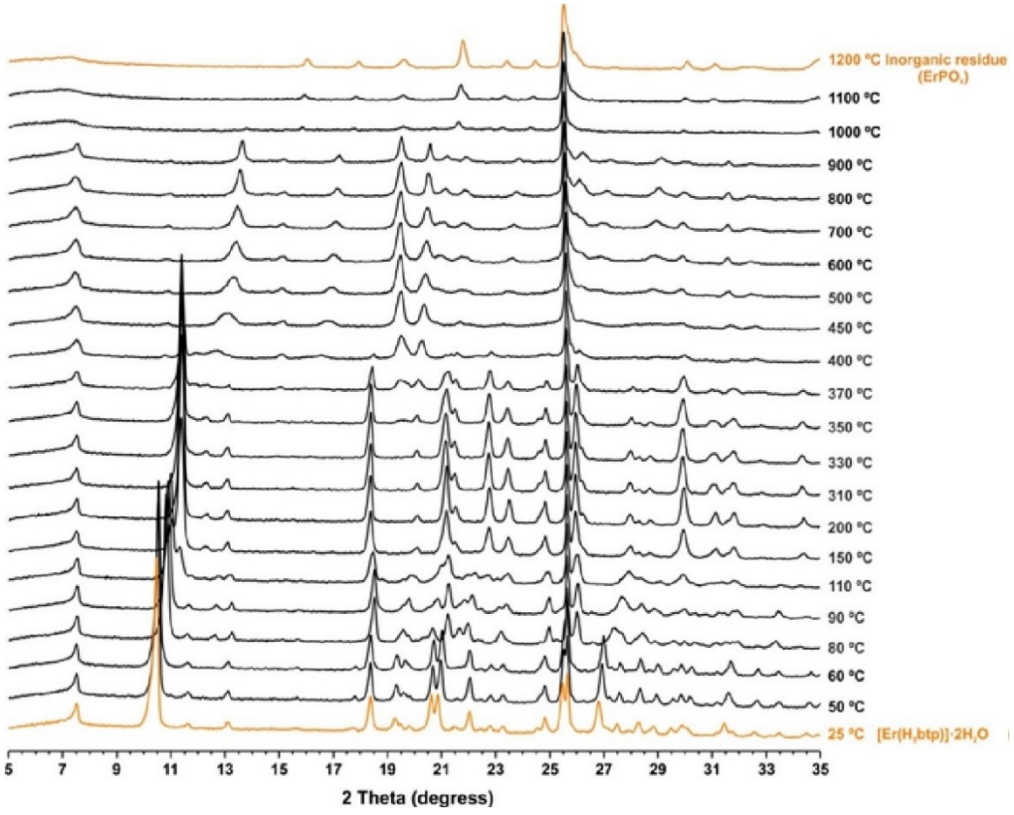

Fig. S30 VTPXRD studies of [Er(H_5btp)]·2H_2O (**1Er**) collected between ambient temperature and *ca.* 1200 ºC.

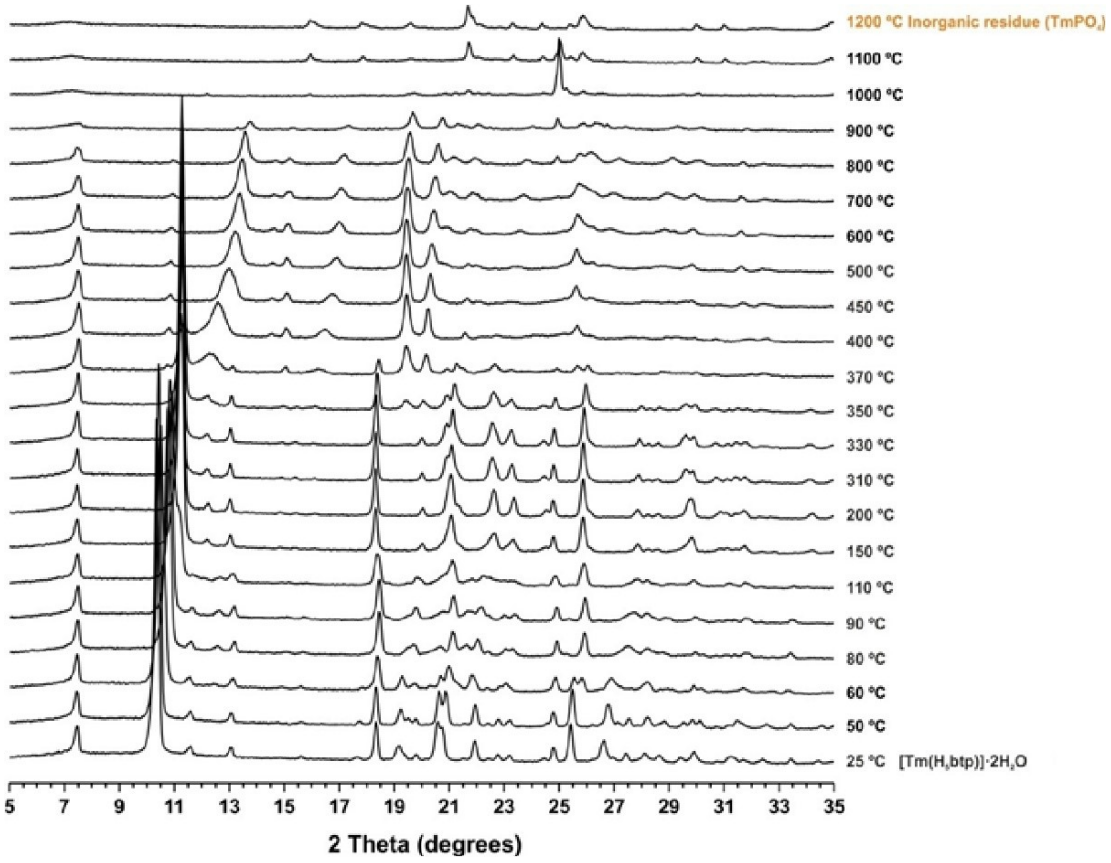

Fig. S31 VTPXRD studies of $[Tm(H_5btp)]\cdot 2H_2O$ (**1Tm**) collected between ambient temperature and *ca.* 1200 ºC.

References

1. A. D. G. Firmino, R. F. Mendes, D. Ananias, S. M. F. Vilela, L. D. Carlos, J. P. C. Tomé, J. Rocha and F. A. A. Paz, Microwave Synthesis of a photoluminescent Metal-Organic Framework based on a rigid tetraphosphonate linker, *Inorg. Chim. Acta*, 2017, **455**, 584-594.
2. A. D. G. Firmino, R. F. Mendes, M. M. Antunes, P. C. Barbosa, S. M. F. Vilela, A. A. Valente, F. M. L. Figueiredo, J. P. C. Tomé and F. A. A. Paz, Robust Multifunctional Yttrium-Based Metal Organic Frameworks with Breathing Effect, *Inorg. Chem.*, 2017, **56**, 1193-1208.
3. T. Kottke and D. Stalke, Crystal Handling at Low-Temperatures, *J. Appl. Crystallogr.*, 1993, **26**, 615-619.
4. APEX2 *Data Collection Software Version 2.1-RC13*, **2006**.
5. SAINT+ Data Integration Engine v. 8.27b©, **1997-2012**.
6. L. Krause, R. Herbst-Irmer, S. G.M. and S. D, SADABS 2016/2, **2015**, **48**, 3-10.
7. G. M. Sheldrick, A short history of SHELX, *Acta Crystallogr. Sect. A*, 2008, **64**, 112-122.
8. G. M. Sheldrick, SHELXL Version 2017, Program for Crystal Structure Refinement, **2017**.
9. C. B. Hubschle, G. M. Sheldrick and B. Dittrich, ShelXle: a Qt graphical user interface for SHELXL, *J. Appl. Crystallogr.*, 2011, **44**, 1281-1284.
10. K. Brandenburg, DIAMOND, Version 3.0a Crystal Impact GbR, **1997-2014**.
11. D. Ananias, A. D. G. Firmino, R. F. Mendes, F. A. A. Paz, M. Nolasco, L. D. Carlos and J. Rocha, Excimer Formation in a Terbium Metal–Organic Framework Assists Luminescence Thermometry, *Chemistry of Materials*, 2017, **29**, 9547-9554.